

Kjell Petersen Synstad

Small-Signal Stability Analysis of GridVille's Microgrid

Master's thesis in Energy and Environmental Engineering

Supervisor: Mohammad Amin

Co-supervisor: Yusuf Shankar Gupta

June 2022

Kjell Petersen Synstad

Small-Signal Stability Analysis of GridVille's Microgrid

Master's thesis in Energy and Environmental Engineering
Supervisor: Mohammad Amin
Co-supervisor: Yusuf Shankar Gupta
June 2022

Norwegian University of Science and Technology
Faculty of Information Technology and Electrical Engineering
Department of Electric Power Engineering

Abstract

The objective of this thesis is to use small-signal analysis on the microgrid of GridVille, a student project trying to build a microgrid for a village in Nepal, to come with practical suggestions for improving the stability of the energy system. The practical suggestions that is mentioned are concretised by investigating changing the parameters voltage, droop gain, interconnecting lines and load distribution.

To analyse the microgrid, the paper *Reduced-order model and stability analysis of low-voltage DC microgrid* by Sandeep Anand and Baylon G. Fernandes was used as the foundation. The model in the paper is recreated and a new model is developed for GridVille's microgrid with the same procedure as the paper. The line currents and source currents have the same response, expect for a difference in the time scaling for the paper recreation. For GridVille representation, the response follows similar patterns compared to the papers response and is therefore used for further analysis.

The results generally show that there are not big variations in position of the rightmost eigenvalue. All the scenarios are stable and well damped. The biggest difference in eigenvalues comes from the scenario where two interconnecting lines are added to the microgrid. There is a significant movement of the rightmost eigenvalue towards the y-axis. The scenario with the rightmost eigenvalue the most to the left is where the scenario where two power sources are placed in one node, and not two different.

The suggestions for improving the GridVille's microgrid is summed up in the points:
1) Increasing the voltage
2) One bigger power source is better than two equally big
3) Reduce the number of nodes. Based on the results, it seems that the system is more stable when the microgrid is simpler. To achieve that, the Battery Energy Storage System (BESS) or loads can be placed on more than one node and power sources can be put together. However, due to the geographical location of the microgrid, this may not be possible if there solar photovoltaic (PV) array and wind turbine do not produce their maximum at the same location or that there only one place that the load can be placed.

Sammendrag

Denne oppgaven har som mål å analysere mikronettet til GridVille, en studentorganisasjon som skal bygge et micronett for en landsby i Nepal, for å komme med praktiske forslag til hvordan å forbedre stabiliteten i energisystemet. De praktiske forslagene som blir nevnt blir konkretisert ved å undersøke effekten av å endre spenningen, statikk, sammenkoblede linjer og fordeling av last.

For å analysere micronettet, ble artikkelen *Reduced-order model and stability analysis of low-voltage DC microgrid* av Sandeep Anand og Baylon G. Fernandes brukt som grunnlag. Modellen i artikkelen ble rekonstruert og en ny modell for GridVille sitt micronett ble utviklet med artikkelen som grunnlag. Linjestrømmene og kildestrømmene har den samme responsen, men tidsaksen er forskjellig mellom artikkelen og den rekonstruerte modellen. For representasjonen av GridVille, så følger responsen et likt mønster sammenlignet med artikkelen og blir derfor brukt for videre analyse.

Resultatene viser at det ikke er store variasjoner i plasseringen til den egenverdien plassert lengst til høyre. Alle scenarioene er godt dempet og har god respons. Den største forskjellen i egenverdier kommer i scenarioet med to ekstra sammenkoblede linjer i micronettet. Da er det en stor forflyttelse av egenverdien som er lengst til høyre mot y-aksen. Scenarioet der egenverdien lengst til høyre er lengst fra y-aksen er når to av energikildene er satt i samme node, og ikke fordelt på to forskjellige.

Forslagene for å forbedre mikronettet til GridVille kan bli oppsummert i punktene: 1) Øke spenningen 2) En større energikilde er bedre enn to like store 3) Reduser antall noder. Basert på resultatene, er tendensen at mikronettet er mer stabilt nå det er simplere. For å oppnå dette, så kan batteriet or lastene bli plassert ut på mer enn bare en node, eller energikilder kan bli satt sammen. Det kan hende at den geografiske plasseringen av mikronettet ikke gjør dette mulig siden kanskje ikke solcelleanlegget og vindturbinen produserer maks ved samme plassering, eller at lasten bare kan bli plassert en plass i landsbyen.

*Høiskolen vil gjøre dere til studerende. Vi, Samfundet, vil
gjøre dere til studenter.*

- Edgar B. Schieldrop

Preface

This master thesis is the final part of the two year master programme Energy and Environmental Engineering at NTNU (*Norges teknisk-naturvitenskaplige universitet*). It is the academic preparation for the master thesis, which is a cooperation with the Engineers Without Borders (IUG) NTNU's project called GridVille. It was supervised by Associate Professor Mohammad Amin and Postdoctoral Fellow Yusuf Shankar Gupta. The communication with GridVille has gone through Project Manager Maurice Sudkamp and Chief Electrical Engineer Varshan Erik Shankar.

There are several I would like to thank for their contribution. Firstly, I would like to thank Professor Mohammad Amin for his guidance through the master thesis. I would like to thank Postdoctoral Fellow Yusuf Shankar Gupta for helping me with everything from calculations and simulations to sorting my thoughts on the thesis. The input and help have been much appreciated.

From GridVille, I would like to thank Project Manager Maurice Sudkamp for making this cooperation possible. Secondly from GridVille, I want to thank the external supervisor, Chief Electrical Engineer Varshan Erik Shankar for being flexible, and the informative meetings and discussions throughout the semester.

Finally, I would like to express my gratitude to Vivas, ISFiT, Studentersamfundet, SIT, UKA, IUG NTNU, Organisasjonskollegiet, my family and friends for the five years of good memories in Trondheim.

Trondheim, 08.06.2022


Kjell Petersen Synstad

Contents

Abstract	i
Sammendrag	ii
Preface	iv
List of Symbols	vii
Abbreviations	viii
List of Figures	ix
1 Introduction	1
1.1 Background	1
1.2 GridVille	1
1.3 Scope and Objective	2
1.4 Outline	3
2 Microgrid Theory	4
2.1 Literature Review	4
2.2 Introduction to Microgrid Theory	4
2.3 Introduction to GridVille’s Microgrid	6
2.4 PV System	7
2.4.1 DC-DC Boost Converter	7
2.4.2 DC-DC Buck Converter	10
2.5 Wind	12
2.6 BESS	13
2.7 Load	15
2.8 Stability Analysis	18
2.8.1 Small-Signal Stability	18
2.8.2 State-Space	18
2.8.3 Participation Factor	19
3 The Model	20
3.1 Base Report Dynamic Equations	20
3.2 Base Report Model	23
3.3 GridVille Representation Dynamic Equations	25

3.4	GridVille Model	26
4	Results	29
4.1	The Base Report	29
4.1.1	Line Current	29
4.1.2	Source Currents	30
4.1.3	Root Locus	31
4.2	GridVille Representation	31
4.2.1	Line Currents	31
4.2.2	Root Locus	32
4.2.3	350 W and 500 W Step in Load	33
4.3	Increasing the Voltage Level	34
4.4	Changing the Droop Gain	35
4.5	Changing the Node Interconnections	38
4.6	Changing the Load Distribution	43
5	Discussion and Conclusion	46
5.1	Comparison to the Paper	46
5.2	Stability Analysis	47
5.2.1	Increasing the Voltage Level	47
5.2.2	Changing the Droop Gain	48
5.2.3	Changing the Node Interconnections	48
5.2.4	Changing the Load Distribution	49
5.3	Further Work	49
5.4	Conclusion	50
	Bibliography	51

List of Symbols

t	s	Seconds in the simulations
i_j	A	Source current at node j
i_{Lj}	A	Load current at node j
i_{jk}	A	Line current from node j to node k
v_j	V	Node voltage at node j
v_j^0	V	Node voltage at node j at zero current
v_{jk}	V	Line voltage from node j to node k
d_j	Ω	Droop gain at node j
g_{lf}	S	Load conductance at node j
l_{jk}	mH	Line inductance from node j to node k
r_{jk}	Ω	Line resistance from node j to node k
v_L	V	Inductor voltage
i_L	V	Inductor current

Abbreviations

BESS	Battery Energy Storage System
CPL	CPL
ESS	Energy Storage System
IUG	Ingeniører uten grenser - Engineers Without Borders
MCC	Microgrid Central Controller
MOSFET	Metal Oxide Semiconductor Field Effect Transistor
MPPT	Maximum Power Point Tracking
NTNU	Norges teknisk-naturvitenskapelige universitet - Norwegian University of Science and Technology
VCO	Voltage Controlled Oscillator
VSC	Voltage Source Converter
VSI	Voltage Source Inverter
PI	Proportional and Integral
PCC	Point of Common Coupling
PLL	Phase Locked Loop
PV	Photovoltaic
PWM	Pulse-Width Modulation
UN	United Nations

List of Figures

2.1	Overview of an example microgrid.	5
2.2	Overview of GridVille’s microgrid.	6
2.3	Boost converter topology.	7
2.4	Inductor voltage and current for a DC-DC boost converter.	8
2.5	Flow chart of the MPPT algorithm.	9
2.6	Output voltage and current for the boost converter with MPPT.	10
2.7	Buck converter topology.	10
2.8	Inductor voltage and current for a DC-DC buck converter.	11
2.9	Voltage control used for the buck converter	12
2.10	Output voltage and current for the buck converter.	12
2.11	Bi-directional buck-boost converter topology	13
2.12	Current controller for the bi-directional buck-boost converter.	14
2.13	Battery and load voltage and current for the buck-boost converter.	14
2.14	Topology of an three-phase inverter.	15
2.15	The PWM characteristics for the DC-AC inverter.	16
2.16	Topology of a current controller.	16
2.17	Load voltage and current for the inverter.	17
3.1	Overview of the microgrid of the paper.	20
3.2	The paper’s state-space simulation process.	22
3.3	The paper’s representation used in Simulink [®]	24
3.4	Overview of the microgrid of GridVille.	25
3.5	GridVille’s state-space simulation process.	26
3.6	GridVilles representation used in Simulink [®]	28
4.1	Response in line currents after a load step for the paper’s microgrid.	30
4.2	Response in source currents after a load step for the paper’s microgrid.	30
4.3	Change in eigenvalues for the paper’s grid.	31
4.4	Response in line currents after a step of 100 W at load 4 for GridVille.	32
4.5	Change in eigenvalues for the GridVille’s grid.	33
4.6	Load step at the load for GridVille.	34
4.7	Load step of 100W with 480 V rated voltage for GridVille.	35
4.8	Load step of 100W with droop set 1 for GridVille.	36

4.9 Load step of 100W with droop set 1 for GridVille. 38

4.10 Overview of the microgrid of GridVille with interconnection set 1. . . 38

4.11 Load step of 100W with interconnection set 1 for GridVille. 40

4.12 Overview of the microgrid of GridVille with interconnection set 2. . . 40

4.13 Load step with interconnection set 2 for GridVille for Simulink. . . . 42

4.14 Load step with interconnection set 2 for GridVille for state-space. . . 42

4.15 Overview of the microgrid of GridVille with load distribution set 1. . . 43

4.16 Load step of 100W with load distribution set 1 for GridVille. 44

4.17 Overview of the microgrid of GridVille with load distribution set 2. . . 44

4.18 Load step of 100W with load distribution set 2 for GridVille. 45

1 Introduction

This is the introductory chapter giving some background information about why this thesis is relevant, both when it comes to the relevance in the academic research and for the GridVille. The chapter ends with the scope and objective of the thesis before the outline of the following chapters are. Chapter 1.2 is taken from the specialisation project[1], but partially changed.

1.1 Background

In a world becoming more reliant and more reliant on electricity and technology, there are still 789 million people in the world living without access to electricity [2]. Electricity is a necessity in everything from agriculture, education, communication, high technology, running basic businesses and healthcare. As a part of the seventh United Nations' (UN) sustainable development goals, clean and affordable for everyone. In a poor country like Nepal, the positive effect the access to electricity has on life quality is immensely. [2, 3]

Supplying this vital electricity to the people with access to electricity, is often a complex transmission grid interconnecting big power producers, industry, households and countries. However, in areas where electricity is scarce and unavailable, these complex transmission lines delivering the power, is often poorly developed and the cost of expanding this grid is expensive [4]. Developing smaller, local grid for communities or households can be an important factor of giving more people access to clean and reliable electricity. This is where microgrids in island mode can be a solution. [4, 5, 6]

Research on topics regarding microgrids, clean energy and energy access are a few topics of many that NTNU have. The goal is that NTNU will contribute to every of the 17 sustainable development goals [7]. And with the slogan "Knowledge for a better world", this area of research fits right in. [8]

1.2 GridVille

This master thesis will consider the stability of the microgrid of GridVille. GridVille is a student project organised by Engineers Without Borders (IUG) NTNU and their ambition is to design, model, build and test a microgrid at NTNU in Trondheim. After that, the ambition is to do the same, with improvements from the first system, at a university in Kathmandu in Nepal. Then, the goal is to design it for the weather conditions closer to the final goal, which is a village in Nepal without access to electricity.

GridVille is a newly started project, which means that everything has to be done for the first time. Everything from the organisation structure to the component design has to be done from the bottom. The master thesis will try to support the work by the volunteers in GridVille to designing a functioning microgrid which can be used

in a community without access to electricity.

GridVille is not only a technical project where engineering students are going to design a microgrid. There are also groups responsible for marketing, an education group responsible for the knowledge exchange, and an analyst group that finds the optimal location and best usage of the microgrid. The project tries to involve relevant subjects at NTNU, such as Design of Wind Turbines, Power Electronics, to name a few, to contribute with their work on the project. GridVille is a project connecting the values of NTNU, and the different study programmes, working together trying to come with solutions and knowledge for a better world.

1.3 Scope and Objective

The project started with the goal of analysing the full GridVille microgrid, with several different converters and power sources. However, after starting on this and simulating the different sources and loads with the converters, too many obstacles occurred for it to be finished in time of the master thesis' deadline. The components in Simulink[®] would not be assembled and working properly. That is why the choice of switching to the small-signal analysis of the microgrid where the converters' output have been assumed to be voltage sources. After that choice was made, the paper *Reduced-order model and stability analysis of low-voltage DC microgrid* [9] by Sandeep Anand and Baylon G. Fernandes was found and the modelling was based on that paper.

The goal of the thesis is to find possible improvements to the microgrid. Using the paper mentioned to suggest improvements on the structure and fundamentals of the microgrid, rather than the specific values of the components. Therefore, the thesis statement can be formulated as:

**Use small-signal analysis on the GridVille microgrid
to come with practical suggestions for improving the
stability of the energy system.**

To quantify what is meant by the "practical suggestions", step response and eigenvalue analysis for the following changes in parameters will be done to see if they could be changed to improve the stability of the microgrid:

- Voltage
- Droop Gain
- Interconnecting lines
- Load Distribution

1.4 Outline

In this report, there will be 5 chapters that consist of:

- **Chapter 2:** Following this introduction chapter, Chapter 2 will present the relevant microgrid theory. It will also go through the initial work with the converters and power sources. The first one is the photovoltaic (PV) system with a boost converter and a buck converter, and it will be explained why it was not taken further in the master thesis. Then, the Battery Energy Storage System (BESS), the bidirectional buck-boost converter will be elaborated and explained why it was not taken further in the thesis. Then, the inverter for the three-phase load is presented. After that, some stability analysis theory will be presented.
- **Chapter 3:** Here, the base report will be presented and recreated. From that report, the GridVille model will be created and the specifications will be presented.
- **Chapter 4:** This chapter will consist of the comparison of the base report and the GridVille representation, and the simulations of the changed voltage, droop setting, node interconnection and load distribution to see if the stability can be improved.
- **Chapter 5:** This chapter will discuss the results and see if there are any suggestions of practical improvements for the microgrid, before discussing some potential improvements for the future thesis and summarising everything in the conclusion.

2 Microgrid Theory

This chapter will elaborate on the basic theory of microgrids, relevant components for the investigated paper and general information about GridVille's microgrid. This will be done by firstly going through some basic microgrid theory before presenting GridVille's microgrid. Then there will be some general information about the different electronics parts, control system and the analysis methods used in this thesis.

The parts chapter 2.2 and 2.3 have not been significantly changed since the specialisation project, and are therefore similar with some improvements. Chapter 2.4, 2.7 and 2.8 has taken paragraphs from the specialisation project, but some new parts are added. [1]

2.1 Literature Review

As a part of the research of the academic field within the theme of the master thesis, some articles was evaluated to get a broader view of the field. The article in [10] looks at the energy management issues for microgrids in island-mode dominated by PV power sources, with BESS and a load. The trade-off between complexity of the grid and the quality is here discussed. Optimisation is a big topic within microgrids, and [11] reviews different optimisation techniques for different criteria, and that states that artificial intelligence becomes important in further microgrid optimisation research. Another paper, [12] focuses on optimising microgrids sustainably when different stakeholders are considered.

As the specialisation project was focused to gain experience with a AC microgrid instead of a DC microgrid, there were some paper evaluated in the early stages about the grid connected microgrids as well. The article which the specialisation project was based, [13], focused on AC and DC active damping in a AC Grid connected to a HVDC line to a offshore wind farm. For the strategies if a grid connected microgrid suddenly have to operate in island mode, the article [14] looks at different control strategies for these instances. For the modelling and tuning of the inverters in a microgrid, the articles [15] and [16] give a good understanding of the issues and approaches.

2.2 Introduction to Microgrid Theory

This chapter will consider more of the fundamental microgrid concepts needed for this thesis. One definition of a microgrid is that it is a network of power production units, loads and often energy storage that operate either isolated, island mode, or integrated to a power grid. The size of a microgrid vary between a few kilowatts to several megawatts, voltages may vary from from 400 volts to some kilovolts, and there are many different configurations of energy sources and sizing. [17, 18]

Their function could either be to operate without any interaction from other grids, constantly connected or operate connected to a grid and have the ability to run a time interval isolated. Regardless of the function, a well tuned control system to balance the unregulated power from renewable energy sources, power electronic devices, energy storage systems and load profiles, is crucial. [17, 18]

Figure 2.1 shows an example of a microgrid connected to the utility grid through a point of common coupling (PCC) breaker with a load, synchronous generator, energy storage system (ESS), wind turbine and solar PV panels. The grid, load and synchronous generator at the top of the figure, are the traditional components in the grid, while the power electronics based power sources as ESS, wind turbines and solar PV panels at the bottom are relatively new in the power grid. The black lines show the electrical feeder between all the parts and the red, dotted lines show the control and communication link between the measurements on the electrical components, measurements and the control system. The primary control works on each power unit, while the microgrid central controller (MCC) controlling the microgrid system. There may also be communication with the external utility grid to either export electricity from the microgrid or import to the microgrid. [17, 19]

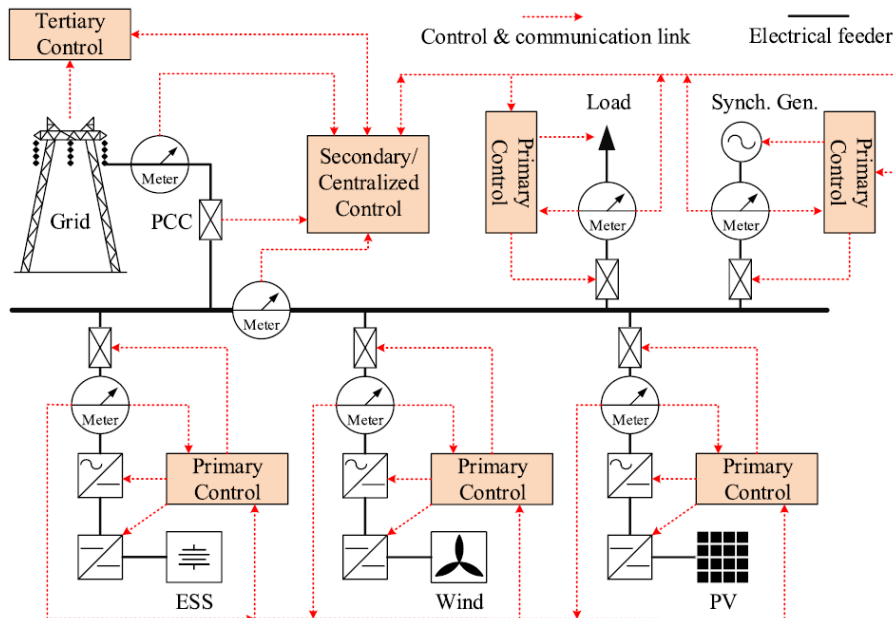


Figure 2.1: Overview of an example microgrid. [19]

The microgrid control system consists of both the software that calculates the signals and the hardware that receive and send signals to the electrical devices. The objective of the control system is split into four main categories:

- Voltage, current and frequency stability.
- Balancing demand and supply of power.
- Economic dispatch calculations and demand side management.
- Switching operation modes.

Where the last two points are not applied for microgrids only operating in island mode. [19]

As the main purposes for the control system of a microgrid is to keep the voltages, currents and frequency stable and within an acceptable range, and balancing production and consumption, primary control for each component plays a key role in keeping the system stable. Since the grid keeps the voltage and frequency stable, island mode microgrids, especially inverter-based, are very challenging of operating compared to when connected to the grid. Fast voltage and current control loops in addition to a phase-locked loop (PLL) are required for a well functioning microgrid. [19, 20]

2.3 Introduction to GridVille's Microgrid

The planned GridVille microgrid that this thesis is based on can be seen in Figure 2.2. The four main power components are a wind turbine, solar PV array, a battery and a load. All the components are connected to the power box which includes the power electronic parts with the corresponding primary control system and a MCC.

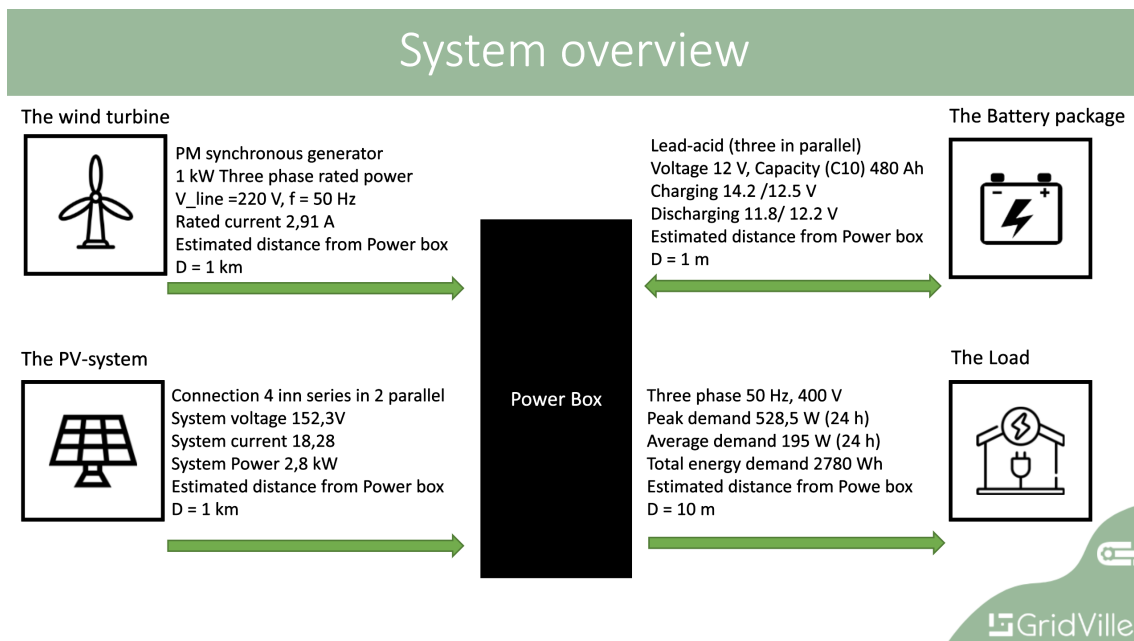


Figure 2.2: Overview of GridVille's microgrid. [21]

The wind turbine uses a three-phase synchronous generator connected to a transformer. That transformer is connected to a AC-DC rectifier and a DC-DC converter which is connected to the common DC bus. For the solar PV panels, it is only connected to a DC-DC converter and onto the DC bus. The battery uses a bidirectional DC-DC converter to connect it to the DC bus. For the single-phase AC load, it is connected to a transformer which is connected to a DC-AC inverter.

2.4 PV System

This chapter will first consider the basic boost converter theory, then describe the maximum power point tracking (MPPT) control for the PV array representation in Simulink[®] and the ending with an explanation about why the it was not taken further for the simulations.

2.4.1 DC-DC Boost Converter

DC-DC converters are commonly used for regulating output voltage for electrical applications as DC loads. They are used since the input voltage could be unregulated and fluctuating, whilst the end product of the voltage needs to be stable and regulated. [22]

There are several topologies with different purposes. There are the step-up (boost), step down (buck), a combined step-up and step-down (buck-boost), Cúk and full-bridge converter. This project will only consider the boost converter as it is the only DC-DC converter used in GridVille. There are some assumptions regarding the converters. The inductive and capacitive losses are neglected, in addition to the switching losses. [22]

To control a general DC-DC converter, one or several switches are used to step up or step down the voltage to a desired level. The ratio between the time the switch is closed, t_{on} , and the time the switch is open, t_{off} , decides the output voltage, where the time period is $T_s = t_{on} + t_{off}$. In Equation 2.1, this relation is described as the duty cycle D in the method called *pulse-width modulation* (PWM). [22]

$$D = \frac{t_{on}}{T_s} \quad (2.1)$$

The topology of a boost converter is shown in Figure 2.3. As the name implies, the function of the boost, or step-up, converter is to increase the output voltage V compared to the input voltage V_s . This is done by that when the switch is on, the diode becomes reverse biased, resulting in that the output stage is isolated and the input voltage supplies energy to the inductor. When the switch is off, the energy supplied to the output is both from the voltage source and the inductor. The capacitor is assumed to be relatively large, giving a constant output voltage. [22]

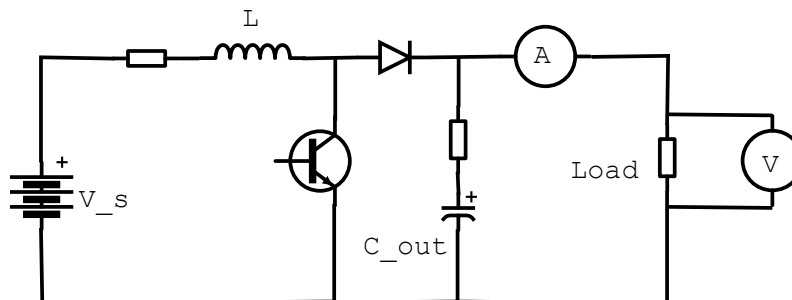


Figure 2.3: Boost converter topology.

The resulting voltage and current across the inductor can be seen in Figure 2.4a and 2.4b. The inductor voltage v_L switches between being equal the source voltage V_s when the switch is on and $V_s - V$ when the switch is off. During t_{on} when the switch is on, the inductor current i_L increases, and when the switch turns off, the inductor discharges and goes decreases until the switch turns on again. The average inductor current I_L is indicated with the dotted line. [22]

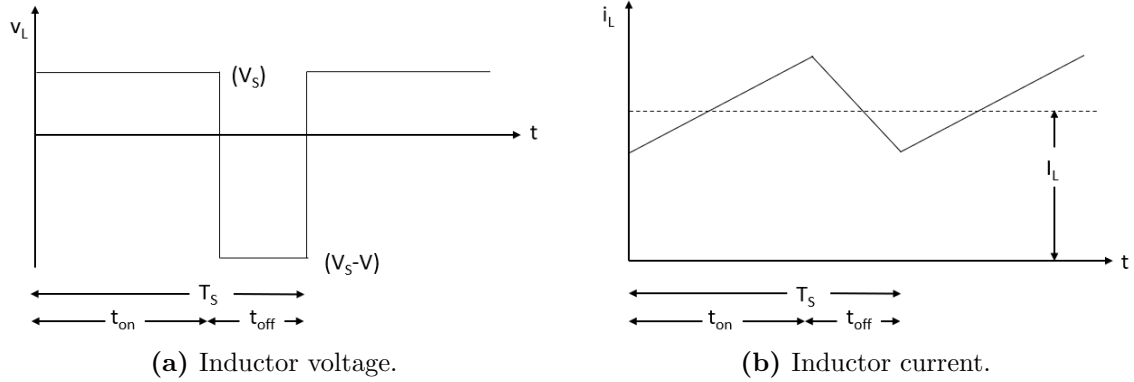


Figure 2.4: Inductor voltage and current for a DC-DC boost converter. [22]

For boost converters operating in continuous-conduction mode, meaning the inductor current i_L is over zero at all times, Equation 2.2 shows the voltage over the inductor over one time period T_s . [22]

$$V_d t_{on} + (V_d - V_o) t_{off} = 0 \quad (2.2)$$

To find the duty cycle D , Equation 2.2 is divided by time period T_s on both sides and rearranging, Equation 2.3 is found. [22]

$$\frac{V_o}{V_d} = \frac{T_s}{t_{off}} = \frac{1}{1 - D} \quad (2.3)$$

The duty cycle D can then be expressed as Equation 2.4. [22]

$$D = 1 - \frac{V_d}{V_o} \quad (2.4)$$

The values used in the Simulink[®] file is presented in Table 2.1.

Table 2.1: Parameters for the boost converter in Simulink[®].

Parameter	Value
PV Voltage [V]	160
Output Voltage [V]	286
Capacitance [F]	$3.3 \cdot 10^{-3}$
Inductance [H]	$5 \cdot 10^{-3}$

To control the duty cycle to achieve the highest power output from the PV array, MPPT control on the converter is used. The algorithm used is shown in Figure 2.5. It changes the duty cycle up or down when certain criteria for the voltage and currents are met. This algorithm ensures that the maximum power from the PV array is delivered by changing to the optimum duty cycle. [23]

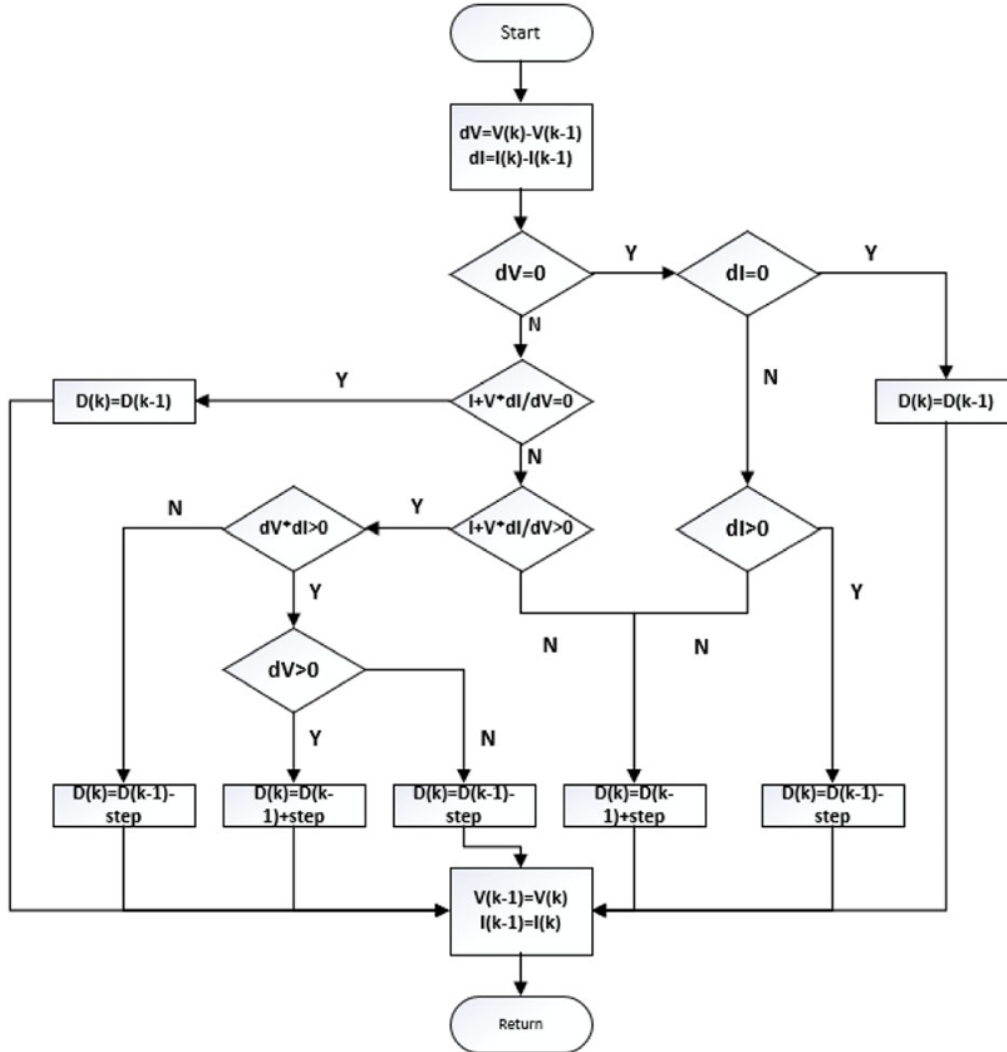


Figure 2.5: Flow chart of the MPPT algorithm. [23]

When running the simulations of the PV array with the boost converter with the MPPT control and the values presented in Table 2.1, the output voltage and current becomes as depicted in Figure 2.6a and 2.6b. The time before both the voltage and current reaches its steady state value is approximately 1.5 seconds. The voltage reaches a value of 286 V and the current reaches 14.3 A. For the output ripple ΔV , it is only 0.8 V, and the output ripple ΔI is 0.04 A.

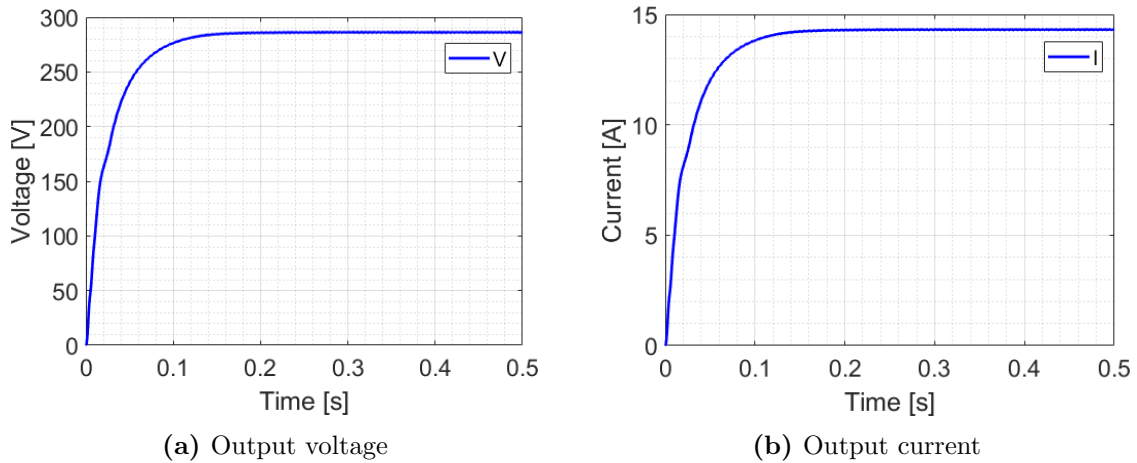


Figure 2.6: Output voltage and current for the boost converter with MPPT.

The response of the voltage and current from the PV array through the boost converter with the MPPT, connecting this converter with the other converter in the microgrid did manage to work properly. The voltage shown in the plots are not the ones that was tried when connecting the converters. Then it was 48 V, as in described previously. After some time trying to solve the issues with the non-working connected converter microgrid. The choice was then to shift focus to another approach for the analysis and the choice of using the base report [9] was made. This ensured that the GridVille microgrid could be analysed and that some possible improvements could be suggested, even though that the method in the paper is simplified and assumes that the converters are modelled as voltage sources with droop control.

2.4.2 DC-DC Buck Converter

Figure 2.7 shows the topology of a buck converter which decreases the output voltage V compared to the input voltage V_s by turning the switch on and off at a certain duty cycle D . When the switch is on, the current flows through the inductor with the input voltage V_s as the voltage source. When the switch is off, the inductor supplies the becomes the voltage source supplying the load with current. The capacitor is assumed to be relatively large, giving a constant output voltage. [22]

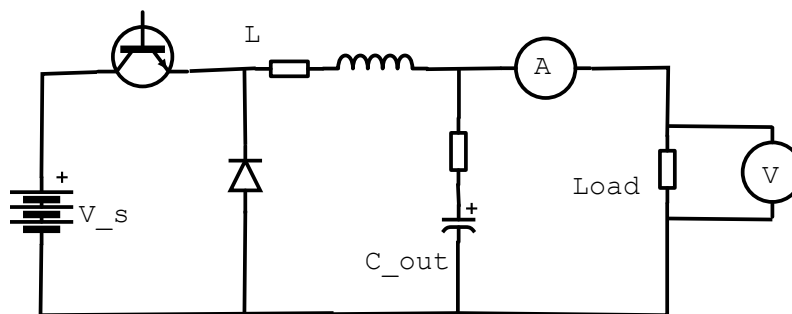


Figure 2.7: Buck converter topology.

For the inductor voltage and current in the buck converter, the behaviour over a time period T_s can be seen in Figure 2.8a and 2.8b. During the time the switch is on, t_{on} , the inductor voltage v_L equals $V_s - V$, and during the time the switch is off t_{off} , the inductor voltage becomes V_s . This voltage results in the inductor current i_L rising during t_{on} and decreases during t_{off} . [22]

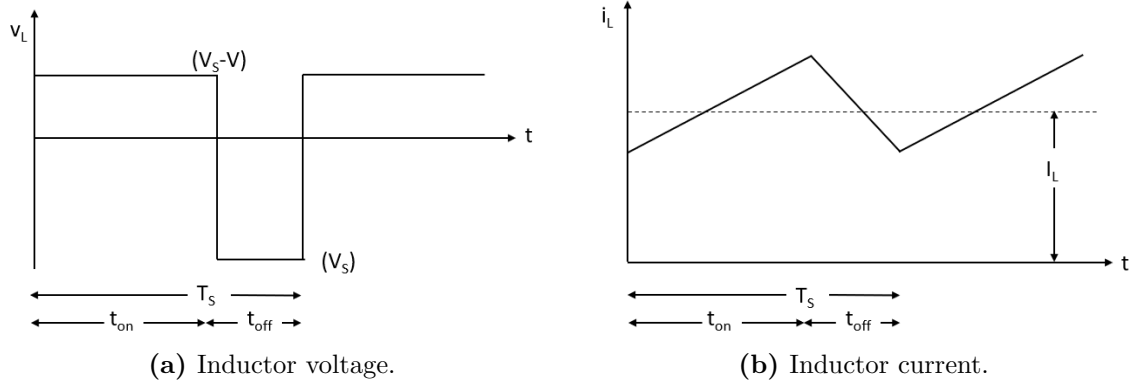


Figure 2.8: Inductor voltage and current for a DC-DC buck converter. [22]

From the areas created in during the time period T_s in Figure 2.8a, the areas over and under the x-axis can be described as in Equation 2.5. [22]

$$(V_d - V_o)t_{on} = V_o(T_s - t_{on}) \quad (2.5)$$

Rearranging Equation 2.5, the duty cycle D can be expressed as in Equation 2.6. [22]

$$\frac{V_o}{V_d} = \frac{t_{on}}{T_s} = D \quad (2.6)$$

For the Simulink[®] simulations of the buck converter, the values from Table 2.2 has been used.

Table 2.2: Parameters for the buck converter in Simulink[®].

Parameter	Value
Input Voltage [V]	600
Output Voltage [V]	400
Capacitance [F]	$3.3 \cdot 10^{-3}$
Inductance [H]	$1 \cdot 10^{-3}$
k_p	$3.75 \cdot 10^{-3}$
k_i	1.25

For the control of the duty cycle D of the buck converter, the proportional gain k_p and integral gain k_i are used in the voltage controller showed in Figure 2.9. Here,

the reference output voltage V_{ref} is subtracted the measured voltage V . That value goes through a PI controller and goes to a PWM generator which generates a signal for the switch. [24]

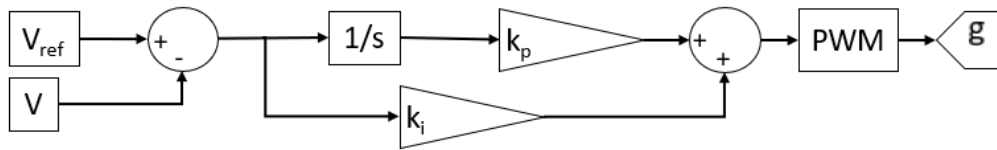


Figure 2.9: Voltage control used for the buck converter

The resulting output voltage and current can be seen in Figure 2.10a and 2.10b. It reaches the desired output voltage very quickly, but there is some noise in the before 0.1 s and after 0.3 seconds. The same trend can be found in the output current.

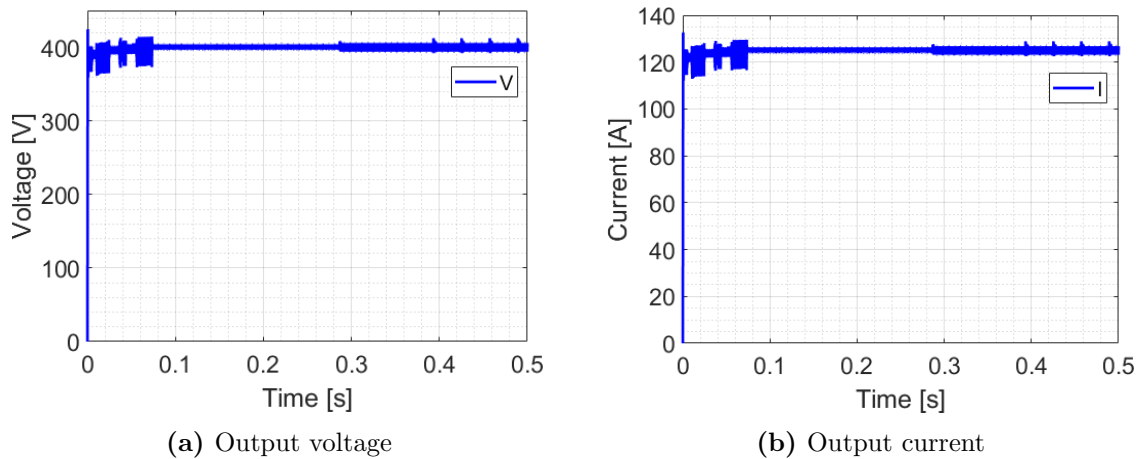


Figure 2.10: Output voltage and current for the buck converter.

The response from the buck converter is faster than the boost converter, but is More noisy. As mentioned when discussing the boost converter, when connecting all the converters together, the microgrid did not work as intended. The When using a voltage closer to 300 V as for the boost converter, the noise became more dominant, therefore the 400 V output is chosen.

2.5 Wind

As there is no wind turbine block in Simulink[®] as for the PV array, the making of the rectifier and buck converter for the wind turbine representation was not started on before deciding to switch focus over to the new analysis method. However, the elaboration of the buck converter in chapter 2.4.2 is relevant, where the input voltage would be rectified from the wind turbine.

2.6 BESS

The bi-directional buck-boost converter shown in Figure 2.11 is used for the battery representation in Simulink[®]. Here, V_s is the battery which is at a lower voltage level than the voltage V_{load} . When power is supplied to the grid, the voltage is stepped up to the voltage level at the grid from the battery. The flow of current is determined by the switching of switch 1 and 2. [22]

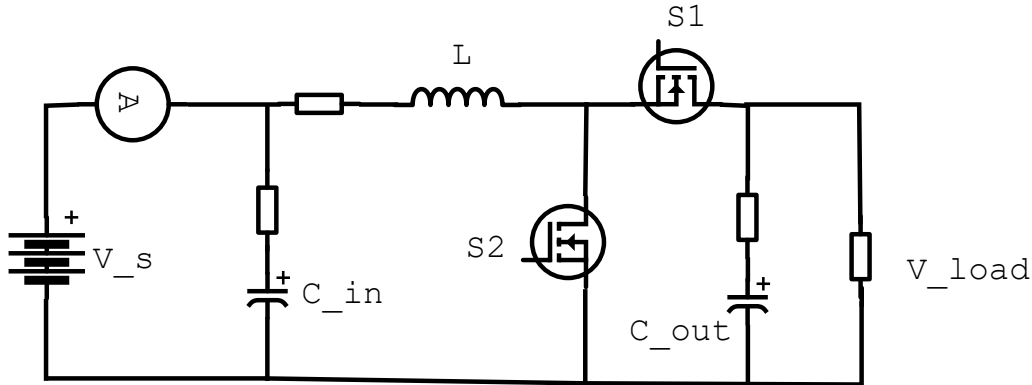


Figure 2.11: Bi-directional buck-boost converter topology

Table 2.3 shows the values used in the bi-directional buck-boost converter.

Table 2.3: Parameters for the buck-boost converter in Simulink[®].

Parameter	Value
Battery Voltage [V]	360
Output Voltage [V]	800
Capacitance in [F]	$20 \cdot 10^{-6}$
Capacitance out [F]	$1 \cdot 10^{-3}$
Inductance [H]	$13 \cdot 10^{-3}$
k_p	1.5
k_i	25

For the controller of the converter, the proportional gain k_p and integral gain k_i is used in a PI controller in the current controller seen in Figure 2.12. The reference current I_{ref} is set, which is negative for charging and positive for discharging of the battery, is subtracted the measured current. However, as the summation block will change the polarity of the two inputs if the reference current is negative. That signal goes through a PI controller and into a PWM generator. This PWM generator gives a signal for switch 1 in Figure 2.11 and the opposite signal for switch 2 if the reference current is positive. If the reference current is negative, witch 2 gets the normal signal and switch 1 the opposite of switch 2. [24]

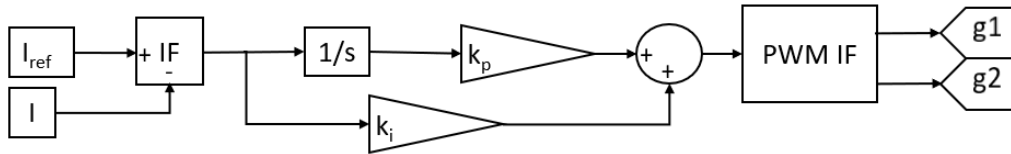


Figure 2.12: Current controller for the bi-directional buck-boost converter.

The response of the converter can be seen for the voltage and current of the battery and grid in Figure 2.13a and 2.13b. The battery voltage slowly increases around 360 V as the battery charges at a current of 25 A before 1 s. After 1 s, the battery discharges and delivers power to the grid. The voltage then slowly decreases and the current is positive 25 A. For the load, the grid voltage is constant at 800 V and changes between positive when delivering and negative when receiving power, with an average of 11.25 A, which means that $P_{in} = P_{out}$.

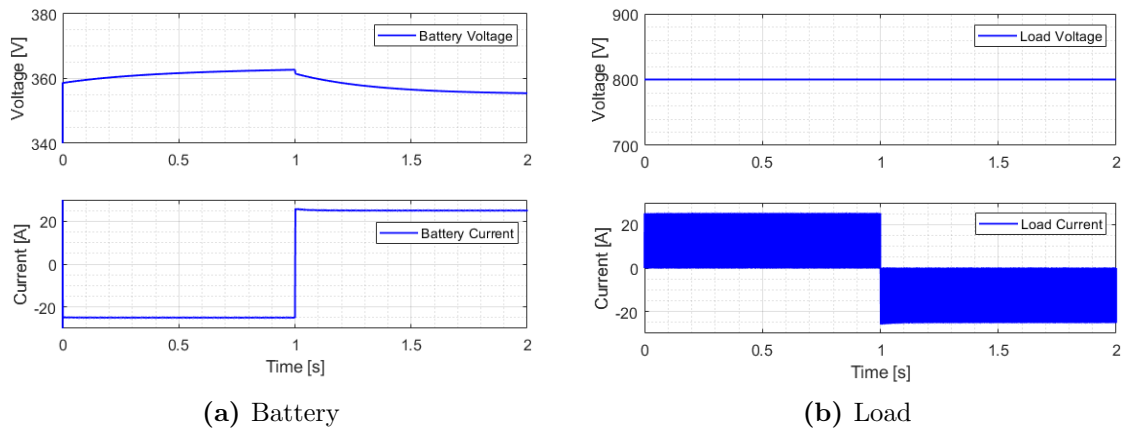


Figure 2.13: Battery and load voltage and current for the buck-boost converter.

The voltage controller that was tried developed for the converter, did not work. The current controller work as it should and was presented. The load current could maybe be evened out with an inductor for a smoother DC current on the load side. As mentioned earlier, the connecting of the converters in the grid did not work properly. However, each converter with different control is shown and tested individually.

2.7 Load

This chapter considers the AC load which is connected to the DC grid through a three-phase DC-AC inverter. The basic principle of an inverter is to transform DC voltage to AC voltage where both magnitude and frequency can be controlled. Inverters are used for constant AC power supply or constant AC loads. These are also called voltage source converters (VSC) or voltage source inverter (VSI). In this project, PWM will be used to control the VSC. Then, the DC input is constant and the VSI controls the magnitude and frequency of the AC output switching done by the PWM. [22, 25]

This PWM signal controls the six switches for the three legs, one for each phase, in the inverter, presented in Figure 2.14. The output of each leg is dependent on the load current since one of the two switches in each leg always is closed. [22, 25]

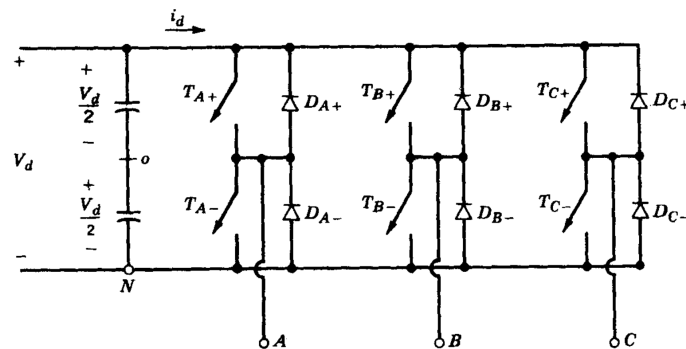


Figure 2.14: Topology of an three-phase inverter. [22]

The PWM tries to obtain balanced three-phase output voltage 120° apart. To do that, a triangular voltage wavefront v_{tri} is compared to a base example of control voltages $v_{control,A,B,C}$ as shown in Figure 2.15b. Any time v_{tri} is higher than the control voltage of each phase, than the output from leg becomes zero. That can be seen in the two phase-to-ground voltages below in Figure 2.15b. The corresponding line-to-line voltage for v_{AB} , shown in Figure 2.15a, giving the sinusoidal v_{LL1} .

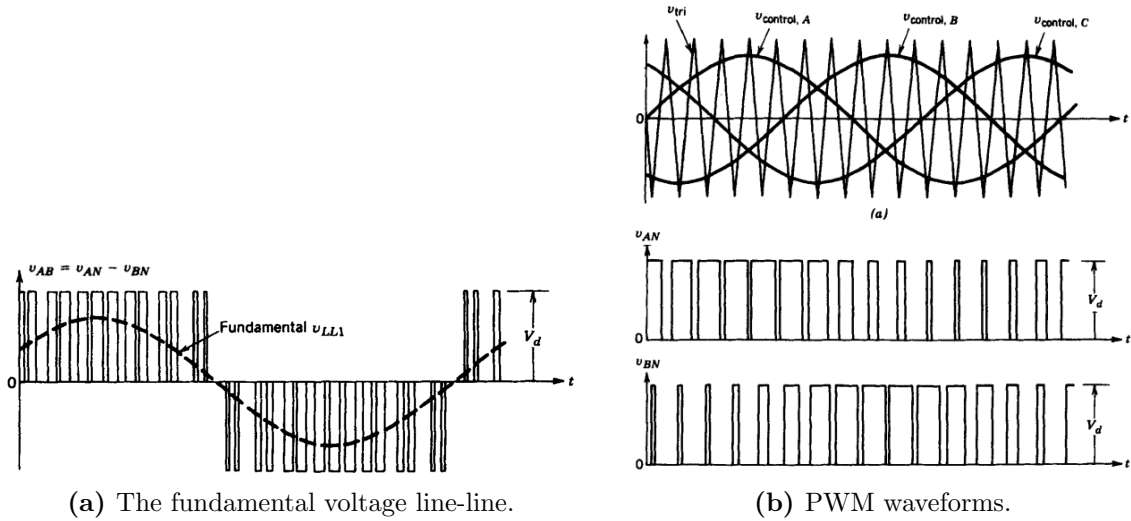


Figure 2.15: The PWM characteristics for the DC-AC inverter. [22]

The signal that is used as reference for the PWM generator, is a basic current controller is shown in Figure 2.16. It takes the active and reactive reference current components $i_{d,ref}$ and $i_{q,ref}$ and subtracts the measured line currents $i_{L,d}$ and $i_{L,q}$, which is measured at the output LCL-filter of the inverter. That sum is sent through a PI controller. In the PI controller, the signals go through a proportional gain k_p and an integral gain k_i . That resulting signals go to a summation block where the output voltage v_{od} and v_{oq} are added. The filter inductance L_c is multiplied with the measured current and the PLL frequency ω_{pll} and is subtracted for the d component and added for the q component. That results in the reference line voltage $v_{cv,ref}$ that is split into the g_d and g_q for the PWM signal. [24]

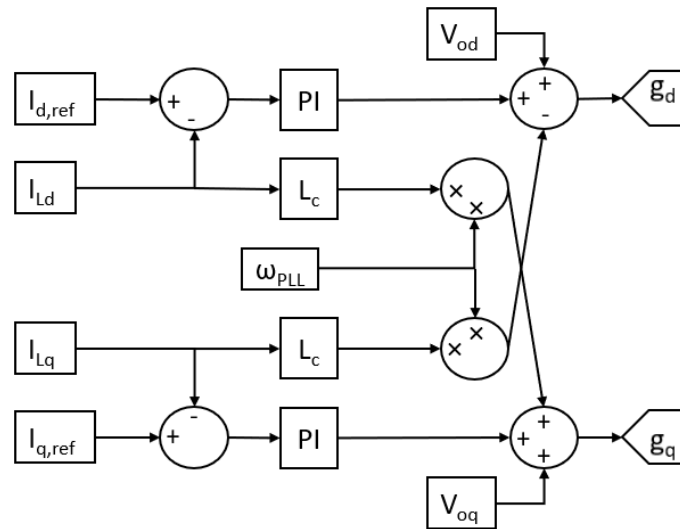


Figure 2.16: Topology of a current controller. [26]

Table 2.4 shows the parameters used in the inverter and LCL-filter.

Table 2.4: Parameters for the inverter in Simulink[®].

Parameter	Value
DC Voltage [V]	360
Capacitance [F]	$40 \cdot 10^{-6}$
Inductance in [H]	$6.6 \cdot 10^{-3}$
Inductance out [H]	$8.25 \cdot 10^{-4}$
k_p	15
k_i	200
ω_{pll}	$2 \cdot 50 \cdot \pi$

The output voltage and current can be found in Figure 2.17a and 2.17b. Since the load in Simulink[®] is the AC load block, the voltage curves are close to perfect. However, the current are disturbed a bit and could use some better filtering from the LCL-filter.

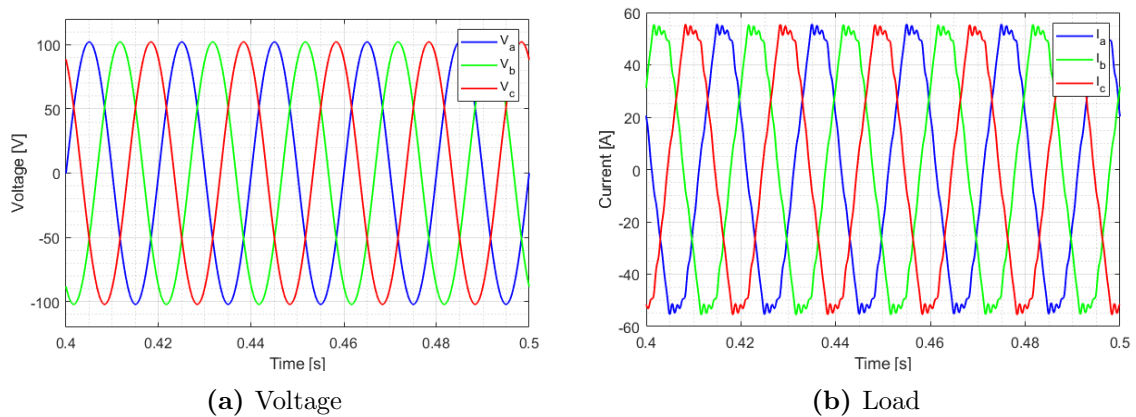


Figure 2.17: Load voltage and current for the inverter.

The responses for the voltage and current is not perfect, but would have been further tuned if the first approach of the thesis had been executed. It would also be implemented a voltage controller to determine the input to the current controller. However, the concept is shown and proven that it works separately, but not in the connected grid.

2.8 Stability Analysis

This chapter will consider the most essential information about the stability analysis tools used in this thesis.

2.8.1 Small-Signal Stability

Small-signal stability analysis is used for state space models. With all the system dynamic equations, they can be linearised when making the right assumptions e.g., signal deviations from the steady-state operating point are minimal. This enables linear techniques to calculate and investigate relevant sensitivity information to see which factors that are affecting the stability of the system. [20, 27]

When all the dynamic equations have been linearised, the eigenvalues of the system can be calculated. After a full small-signal state-space model of the power system is established, its eigenvalues can be calculated. They indicate the damping and frequency of the oscillatory terms, speed of the non-oscillatory ones, which is described in the dynamic response. It is also possible, with further examination, to establish the relationship between the stability and system parameters. [26, 27]

In addition, root locus analysis is often used where the eigenvalues of interest are those close to the right-half plane which are those who represent the slow or poorly damped response. When changing the parameters, it is possible to see the movement of the eigenvalues and see if the system moves toward a more stable or less stable path. [26, 27]

2.8.2 State-Space

For a complex linear system, first-order differential equations or transfer functions can be used to describe the system behaviour [28]. The form is often as presented in Equation 2.7, where the $\dot{\mathbf{x}}$ is the state variables in the dimension $n \times 1$, \mathbf{A} is the state matrix in the dimension $n \times n$, \mathbf{u} is the input in the dimension $r \times 1$, \mathbf{B} is the input matrix in the dimension $n \times r$, \mathbf{y} is the output in the dimension $m \times 1$, \mathbf{C} is the output matrix in the dimension $m \times n$, and \mathbf{D} is the direct transition in the dimension $m \times r$. Here, n is the number of state variables, r is the number of input, and m is the number of outputs. [20, 28, 29]

$$\begin{aligned}\dot{\mathbf{x}} &= \mathbf{Ax} + \mathbf{Bu} \\ \mathbf{y} &= \mathbf{Cx} + \mathbf{Du}\end{aligned}\tag{2.7}$$

2.8.3 Participation Factor

Participation factor is used to describe the effect a state variable in a dynamic system. It says something about to which degree the state variable affect one specific eigenvalue, also called mode. It is used to see to analyse a system without considering the whole physical system. For a participation factor matrix pf , where one state affect only the first mode and the second state variable only affect the second mode, the result would become as presented in Equation 2.8. [20] [30]

$$\mathbf{A} = \begin{bmatrix} 1 & 0 \\ 0 & 1 \end{bmatrix} \quad (2.8)$$

3 The Model

This chapter will present the base report which the GridVille model will be compared to. Firstly, the dynamic equations of the base report will be presented, before the simulations for the base report are recreated and shown. Then, the GridVille model, based on the report's dynamic equations, will be presented, and then compare the results from GridVille with the report. [9]

3.1 Base Report Dynamic Equations

The paper that is going to be the basis for the comparison of the microgrid is "Reduced-order model and stability analysis of low-voltage DC microgrid". In this paper, The microgrid is divided into nodes with both a voltage source and load in each node as depicted in Figure 3.1, with three cables connecting the nodes. [9]

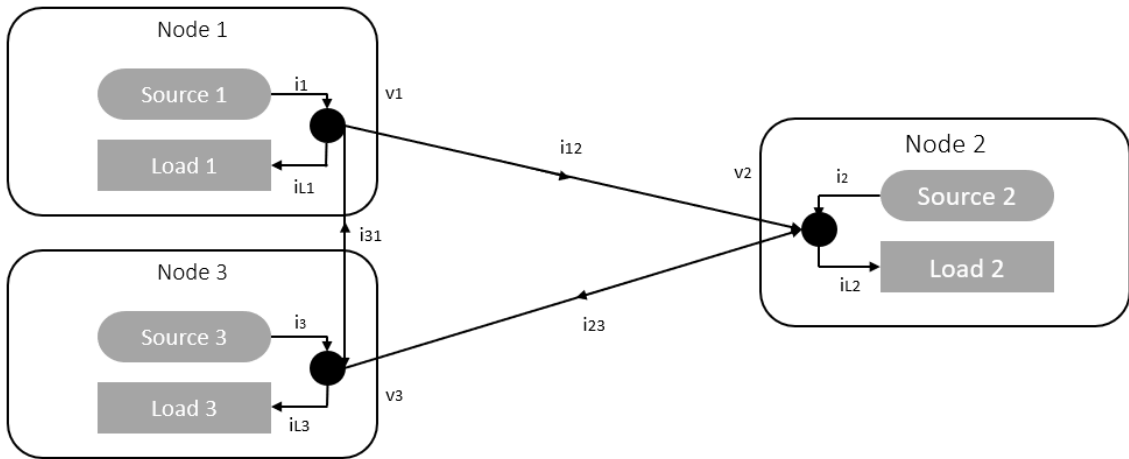


Figure 3.1: Overview of the microgrid of the paper. [9]

The droop equation for source j is described in Equation 3.1, where the reference voltage v_j^{ref} is assumed to be equal to the output voltage v_j . The nominal voltage v_j^0 is the voltage when there is zero current and d_j is the droop gain. [9]

$$v_j = v_j^0 - d_j i_j \quad (3.1)$$

When linearizing Equation 3.1 with small-signal approximation, the output becomes Equation 3.2, where $(\hat{\cdot})$ shows the states' small-signal variation around the operation point. [9]

$$\hat{v}_j = -d_j \hat{i}_j \quad (3.2)$$

Equation 3.2 can be written in matrix form, where $\hat{\mathbf{v}}$ and $\hat{\mathbf{i}}$ are column vectors and \mathbf{D} is a diagonal matrix of droop gains. [9]

$$\hat{\mathbf{v}} = -\mathbf{D}\hat{\mathbf{i}} \quad (3.3)$$

The loads in this paper are constant power loads (CPL), and the load equation is presented in Equation 3.4, where \hat{i}_{lj} is the load current at node j , $-g_{lf}$ is the negative conductance in parallel with a current sink \hat{u}_j . [9]

$$\hat{i}_{lj} = -g_{lf}\hat{v}_j + \hat{u}_j \quad (3.4)$$

When Equation 3.4 is written in matrix form, the result is shown in Equation 3.5. $\hat{\mathbf{i}}_l$ is the column vector of the load currents, \mathbf{G}_l is the diagonal matrix the load conductance of each node and $\hat{\mathbf{u}}$ is the column vector of the current sink at each node. [9]

$$\hat{\mathbf{i}}_l = -\mathbf{G}_l\hat{\mathbf{v}} + \hat{\mathbf{u}} \quad (3.5)$$

To express the dynamics in each line j , Equation 3.6 is presented, where \hat{v}_{bj} is the line voltage, l_{bj} is the line inductance, \hat{i}_{bj} is the line current and r_{bj} is the line resistance. [9]

$$\hat{v}_{bj} = l_{bj}\frac{d\hat{i}_{bj}}{dt} + r_{bj}\hat{i}_{bj} \quad (3.6)$$

Writing Equation 3.6 in matrix form, the result is Equation 3.7 with $\hat{\mathbf{v}}_b$ as the column vector of the line voltages, $\hat{\mathbf{i}}_b$ is the column vector of the line currents, and \mathbf{L}_b and \mathbf{R}_b are the diagonal matrices describing the line inductance and line resistance. [9]

$$\hat{\mathbf{v}}_b = \mathbf{L}_b\frac{d\hat{\mathbf{i}}_b}{dt} + \mathbf{R}_b\hat{\mathbf{i}}_b \quad (3.7)$$

To describe the relationship between the node line voltages $\hat{\mathbf{v}}_b$ and voltages $\hat{\mathbf{v}}$, Kirchhoff's voltage law in matrix form is used and presented in Equation 3.8.

$$\hat{\mathbf{v}}_b = \mathbf{M}\hat{\mathbf{v}} \quad (3.8)$$

Where \mathbf{M} , shown in Equation 3.9, is the incidence matrix with the dimensions $m \times n$, where m is the number of lines and n is the number of nodes. As there are three lines and three nodes, the matrix becomes a 3×3 matrix where the value 1 shows that the line starts at the corresponding node, and -1 show that the line ends up at the corresponding node. [9]

$$\mathbf{M} = \begin{bmatrix} 1 & -1 & 0 \\ 0 & 1 & -1 \\ -1 & 0 & 1 \end{bmatrix} \quad (3.9)$$

Using Kirchoff's current law in matrix form, the relationship between the source currents $\hat{\mathbf{i}}$, load currents $\hat{\mathbf{i}}_l$ and line currents $\hat{\mathbf{i}}_b$ can be expressed. Equation 3.10 shows the relationship, where the incidence matrix \mathbf{M} has been transposed. [9]

$$\hat{\mathbf{i}} - \hat{\mathbf{i}}_l = \mathbf{M}^T \hat{\mathbf{i}}_b \quad (3.10)$$

To describe the system behaviour, Equation 3.3, 3.5, 3.7, 3.8 and 3.10 are combined to form the system equation in Equation 3.11. [9]

$$\frac{d\hat{\mathbf{i}}_b}{dt} = \mathbf{A}\hat{\mathbf{i}}_b + \mathbf{B}\hat{\mathbf{u}} \quad (3.11)$$

Where the \mathbf{A} and \mathbf{B} matrix are expressed as Equation 3.12 and 3.13. [9]

$$\mathbf{A} = -\mathbf{L}_b^{-1} \left(\mathbf{M}(\mathbf{D}^{-1} - \mathbf{G}_l)^{-1} \mathbf{M}^T + \mathbf{R}_b \right) \quad (3.12)$$

$$\mathbf{B} = -\mathbf{L}_b^{-1} \mathbf{M}(\mathbf{D}^{-1} - \mathbf{G}_l)^{-1} \quad (3.13)$$

To simulate the system, the Simulink[®] model in Figure 3.2 is used. The \mathbf{A} and \mathbf{B} matrix are put into the state-space block, which receive the input from one constant block with the value 0 for the loads at Node 1 and 2 and the signal at Node 3 can be changed to represent a step change in the load. The output of the state-space block are divided into each of the three lines and then added the initial values of the line currents, C_1 , C_2 and C_3 , to get the line currents.

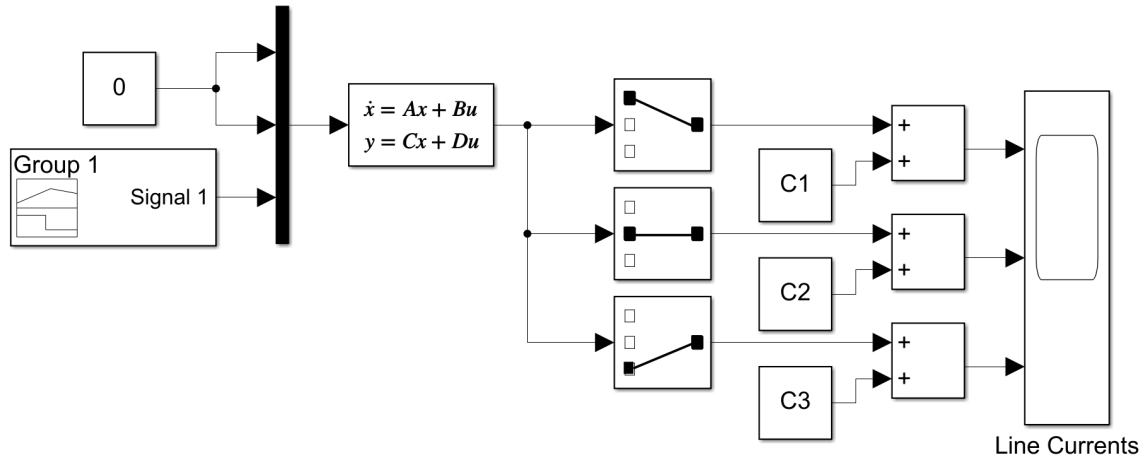


Figure 3.2: The paper's state-space simulation process.

3.2 Base Report Model

The parameters for the three nodes are presented in Table 3.1. All the values are the same for the nodes, except for the load at node 3, which is rated at 70 kW instead of 50 kW. [9]

Table 3.1: Node parameters for the simulated base microgrid. [9]

Parameter	Node 1	Node 2	Node 3
Nominal Voltage [V]	400	400	400
Source Rated Power [kW]	100	100	100
Load Rated Power [kW]	50	50	70
Droop Gains [Ω]	0.04	0.04	0.04

For the values of the lines, the resistance and inductance representing a 1 km long line is presented in Table 3.2.

Table 3.2: Line parameters for the simulated base microgrid. [9]

Parameter	Line 1-2	Line 2-3	Line 3-1
Resistance [Ω]	0.152	0.152	0.152
Inductance [μH]	0.237	0.237	0.237

Using Equation 3.12 and 3.13 with the values from Table 3.1 and 3.2 with the values of incidence matrix \mathbf{M} in Equation 3.9 and load conductance matrix \mathbf{G}_1 , which is found by $(1/(V^2/P_{load}))$.

$$\mathbf{A} = \begin{bmatrix} -983.1758 & 170.9128 & 170.9128 \\ 170.9128 & -983.1758 & 171.7826 \\ 170.9128 & 171.7826 & -983.1758 \end{bmatrix} \quad (3.14)$$

$$\mathbf{B} = \begin{bmatrix} -170.9128 & 170.9128 & 0 \\ 0 & -170.9128 & 171.3466 \\ 170.9128 & 0 & -171.3466 \end{bmatrix} \quad (3.15)$$

Calculating the eigenvalues of the A matrix, the result is the values given in Equation 3.16, which are all in the left half-plane giving a stable system.

$$\lambda_1 = -1155 \quad \lambda_2 = -1154 \quad \lambda_3 = -641 \quad (3.16)$$

The participation factor of the paper's microgrid can be seen in Equation 3.17. It describes the how the different state variables, i_{12} , i_{23} and i_{31} , affect the different

eigenvalues λ_1 , λ_2 and λ_3 . For this system, the first state variable does not have any effect on the first eigenvalues, but affects the second eigenvalue the most and the third with half of that. The second and third state variable affects the three eigenvalues in with the same value. They share the whole contribution for the first eigenvalue, does not affect the second eigenvalue much and share the same effect on the third eigenvalue for the three state variables.

$$\mathbf{pf} = \begin{bmatrix} 0.000 & 0.667 & 0.333 \\ 0.500 & 0.167 & 0.333 \\ 0.500 & 0.167 & 0.333 \end{bmatrix} \quad (3.17)$$

Representing this system in Simulink[®], the following model in Figure 3.3 is used. The three different nodes, which consist of a controllable voltage source and a load, where the load is designed as a CPL. To set the reference voltage V_{j_ref} , where j is the node number, droop control is used where the reference is subtracted the source current multiplied with a droop constant d , where the value of the droop gain can be found in Table 3.1. The load is modelled as a constant power load, the reference current I_{Lj} is set by dividing the rated power by the voltage over the current source, V_{Lj} . All the nodes are connected by lines with a resistance r_{jk} and inductance l_{jk} which the line current i_{jk} goes through, where k is the end node of the line.

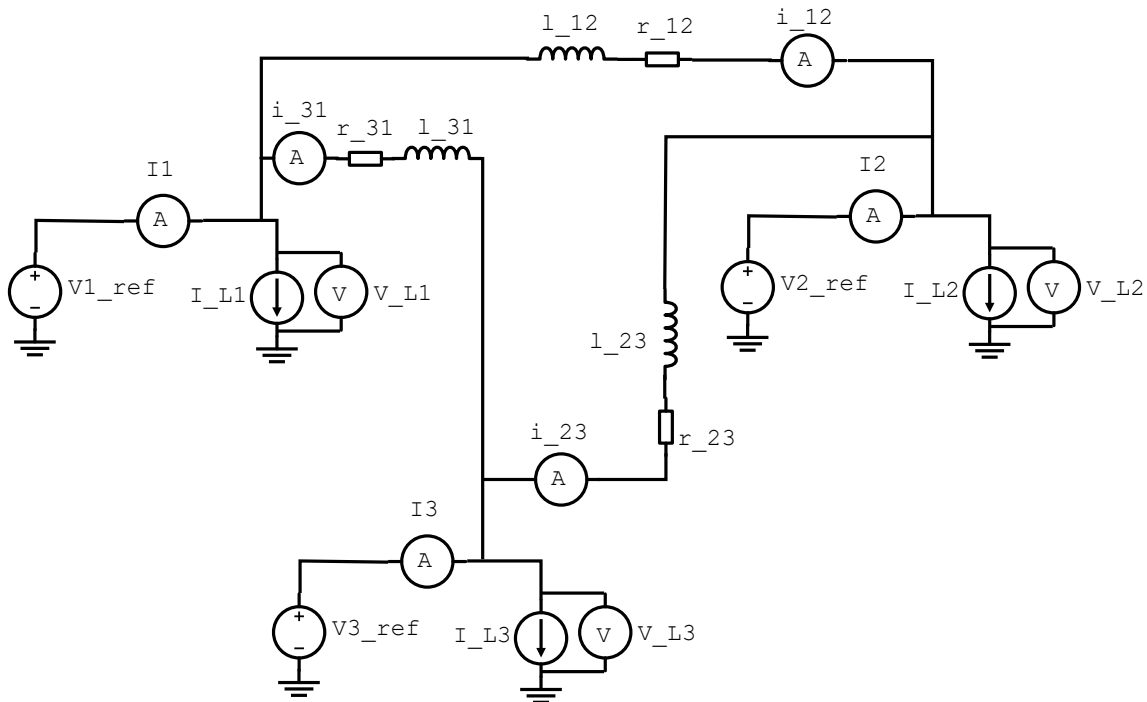


Figure 3.3: The paper's representation used in Simulink[®].

3.3 GridVille Representation Dynamic Equations

When trying to make a representation of GridVille's microgrid from the paper investigated in the previous subchapter, the system overview becomes as depicted in Figure 3.4. Here, there are one additional node compared to the base system in the paper shown in Figure 3.1. Unlike the paper's system, the nodes will only function as a source or load. The BESS node has both a source and load, but will only use the source when it is discharging and only the load when it is charging. Another difference is that the lines are not connected to every node, but the three source nodes are connected to the load node.

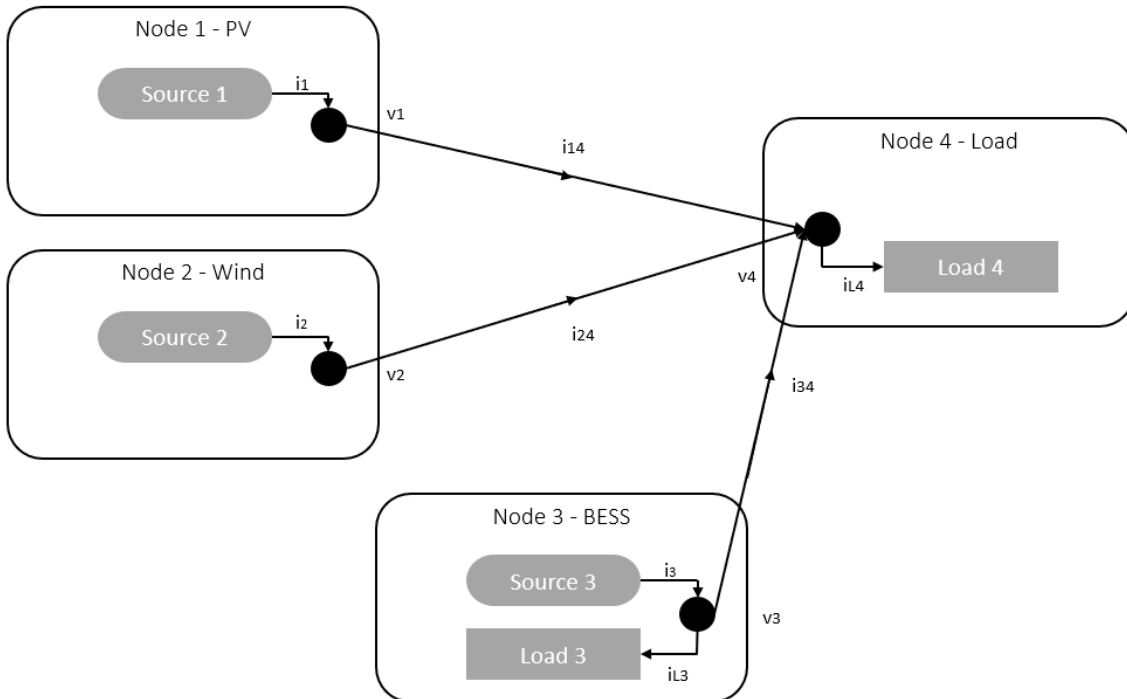


Figure 3.4: Overview of the microgrid of GridVille.

All the equations in subsection 3.1 are equal for this system, but there are some differences in the dimensions of the parameter matrices. All the nodes except the load node have droop control to set the reference, the \mathbf{D} matrix for GridVille showed in Equation 3.18.

$$\mathbf{D} = \begin{bmatrix} d_1 & 0 & 0 & 0 \\ 0 & d_2 & 0 & 0 \\ 0 & 0 & d_3 & 0 \\ 0 & 0 & 0 & d_4 \end{bmatrix} \quad (3.18)$$

The \mathbf{G} matrix in Equation 3.19 will only have two values for node 3 and 4, where g_{l3} will be zero during discharging.

$$\mathbf{G} = \begin{bmatrix} 0 & 0 & 0 & 0 \\ 0 & 0 & 0 & 0 \\ 0 & 0 & g_{l3} & 0 \\ 0 & 0 & 0 & g_{l4} \end{bmatrix} \quad (3.19)$$

The \mathbf{M} matrix, showed in Equation 3.20, shows the indecencies matrix for GridVille.

$$\mathbf{M} = \begin{bmatrix} 1 & 0 & 0 & -1 \\ 0 & 1 & 0 & -1 \\ 0 & 0 & 1 & -1 \end{bmatrix} \quad (3.20)$$

Figure 3.5 shows the state-space model in Simulink[®] representing the GridVille microgrid. The input is zero for the three first nodes, but the signal at the load node can be changed to see the response of the line currents. Then, the state-space block takes the \mathbf{A} and \mathbf{B} from a MATLAB[®] script. The response from for the line currents are then to the initial value, C1, C2 and C3.

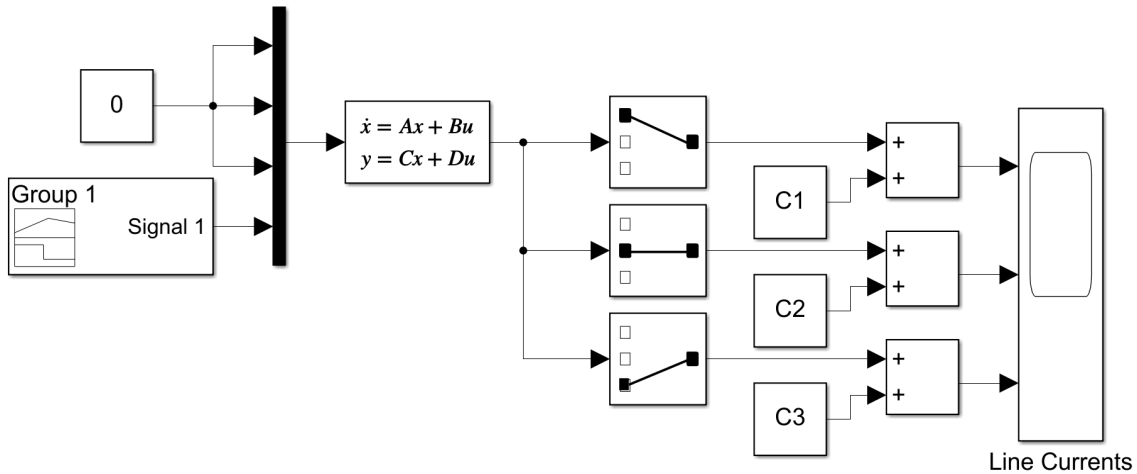


Figure 3.5: GridVille's state-space simulation process.

3.4 GridVille Model

The node parameters for the GridVille microgrid can be found in Table 3.3. The nominal voltage at each node is 48 V, about a tenth of the voltage level in the paper's microgrid. For the rated source power, the values are taken from the GridVille overview in Figure 2.2. The droop values for each node was calculated with the PV rated power at Node 2 as the base with the droop gain at 0.04Ω . Then calculating the maximum current with the equation $I_{max} = \frac{P}{V}$. The maximum current is multiplied with droop gain, and that product should be equal for each node. Therefore, the higher rated power, the lower droop gain, and vice versa. The droop gain at node 4 is set to 1Ω to represent a very small source.

Table 3.3: Node parameters for the simulated GridVille microgrid.

Parameter	Node 1	Node 2	Node 3	Node 4
Nominal Voltage [V]	48	48	48	48
Source Rated Power [W]	1000	2800	576	0
Load Rated Power [W]	0	0	576	500
Droop Gains [Ω]	0.11	0.04	0.19	1

The branch parameters for the GridVille microgrid can be found in Table 3.4 and are the same as in the paper's lines. GridVille are also planning for 1 km of lines from the nodes to the load, and therefore the values have been.

Table 3.4: Line parameters for the simulated GridVille microgrid. [9]

Parameter	Line 1-4	Line 2-4	Line 3-4
Resistance [Ω]	0.152	0.152	0.152
Inductance [mH]	0.237	0.237	0.237

Using Equation 3.12 and 3.13 with the values in Table 3.3 and 3.4 and the values in Equation 3.18, 3.19 and 3.20, the resulting \mathbf{A} and \mathbf{B} matrices are presented in Equation 3.21 and 3.22.

$$\mathbf{A} = \begin{bmatrix} -5904 & -4899 & -4899 \\ -4899 & -5636 & -4899 \\ -4899 & -4899 & -6211 \end{bmatrix} \quad (3.21)$$

$$\mathbf{B} = \begin{bmatrix} -464.1 & 0 & 0 & 5389 \\ 0 & -168.8 & 0 & 5389 \\ 0 & 0 & -801.7 & 5389 \end{bmatrix} \quad (3.22)$$

When calculating the eigenvalues of the \mathbf{A} matrix, the result is showed in Equation 3.23

$$\lambda_1 = -17290 \quad \lambda_2 = -1300 \quad \lambda_3 = -935 \quad (3.23)$$

The participation factor of the paper's microgrid can be seen in Equation 3.24. It describes the how the different state variables, i_{14} , i_{24} and i_{34} , affect the different eigenvalues λ_1 , λ_2 and λ_3 . Since the line current equals the source current for GridVille, i_{14} , i_{24} and i_{34} will be called i_{Wind} , i_{PV} and i_{BESS} for simplicity. For this system, the first state variable affect the three eigenvalues equally. The second and third state variable affects the first eigenvalue the same as the first state variable. They have opposite affect on eigenvalue 2 and three, where state variable two has

the most affect in eigenvalue three and third state variable has the most effect on state variable the second eigenvalue.

$$\mathbf{pf} = \begin{bmatrix} 0.333 & 0.332 & 0.335 \\ 0.321 & 0.052 & 0.627 \\ 0.346 & 0.616 & 0.038 \end{bmatrix} \quad (3.24)$$

Figure 3.6 show the Simulink[®] model of the GridVille microgrid. The blue areas represent each of the nodes, wind turbine, solar PV array, BESS and load, in the GridVille microgrid. For the node except the load node, there is a controllable voltage source With droop control, the model for the paper in Figure 3.3. The constant power loads are removed from each node and the load node has resistive loads instead. Varying the amount of power in the load, breakers are used to change the circuit. The reason for removing the constant power loads is that they would not work in the new setup due to division by zero errors when starting the simulations. In addition, the breaker block for DC circuits in Simulink[®] does not work in the MATLAB[®] 2021b version. Therefore, the breaker consist of two MOSFETs with opposite direction with a gate signal to open and close the breaker.

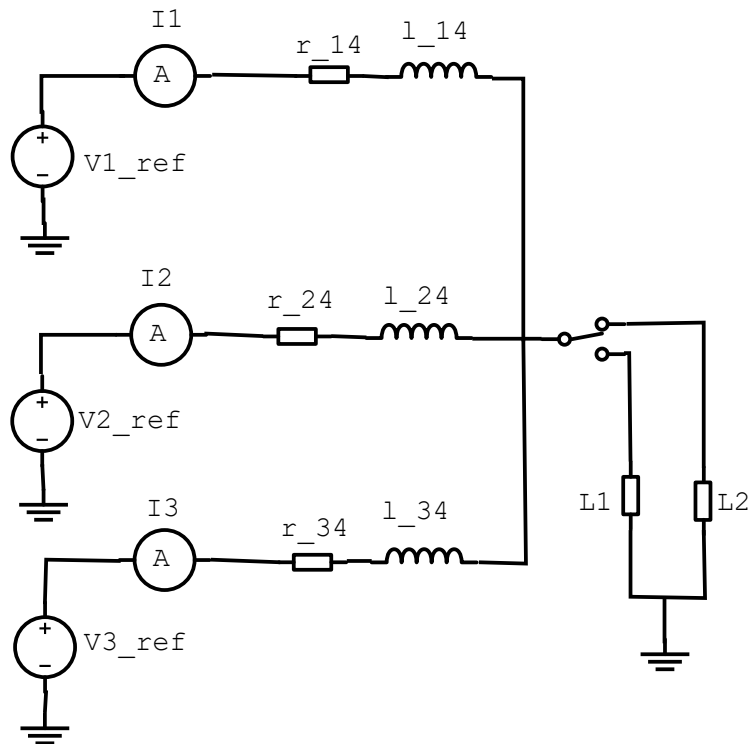


Figure 3.6: GridVilles representation used in Simulink[®].

4 Results

This chapter first go through the simulations of the base report, before replicating the same simulations with the GridVille model. After that, four parameters will be changes to see if there are some effects on the stability of the system.

For all the simulations in this chapter there will be a difference in the time scale on the plots. For the state-space simulations, the plots will have a time scale of 0.02 seconds, while the Simulink simulations will have a time scale of 2 seconds. The reason for this difference is not known, but as the shape and response for the two different model are approximately the same, they are still compared to each other.

In the simulations of GridVille for the different cases, the line currents will be called i_{Wind} , i_{PV} and i_{BESS} . For the cases where the node interconnection and load distribution have been changed and not corresponding to the source current, the line currents are called by i_{jk} , to describe which nodes the currents are going through.

4.1 The Base Report

This chapter will replicate the results from the base paper for the line currents, both for state-space and simulink simulations, source currents and eigenvalues. The goal is to find out if the state-space representation and simulink model are producing the same results and then be able to compare it to the GridVille microgrid in subsection 4.2.

4.1.1 Line Current

The first simulation to be run is the line current response to a step of 10 kW, from 60 kW to 70 kW then 70 kW to 60 kW, at the load at node 3. In Figure 4.1a, the state-space representation of the three line currents are shown. The shape of the responses are similar to the one in the paper . However, the magnitude of the step response is lower than the graphs show in the paper. For the timing of the step, it lasts longer than in the paper to fit the scale of the Simulink response. Therefore, the step lasts for 0.01 seconds rather than 0.1 seconds.

In Figure 4.1b, the Simulink model is run to see the response of the load currents to the same step. Here, the simulation time is much longer than the state-space representation. The line currents use longer time to reach its new steady state value. Therefore, the step lasts for 1 second, which is longer than the simulations in the paper of 0.1 seconds. The magnitude of the response is more similar to the one in the paper.

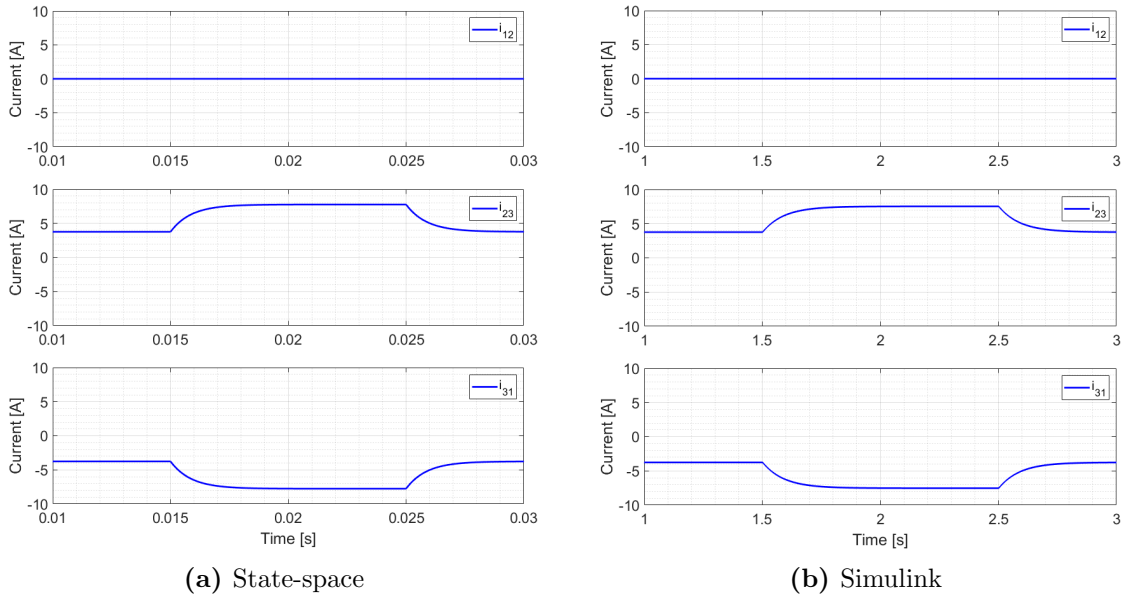


Figure 4.1: Response in line currents after a step of 10 kW at load 3 for the paper's microgrid.

4.1.2 Source Currents

When looking at the response of the source currents for the same step, a step of 10 kW, from 60 kW to 70 kW then 70 kW to 60 kW, at the load at node 3. Figure 4.2 show the response of the source currents at each node. The Source at node 3 has a higher initial current of approximately 145 A, while node 1 and 2 have the same source current of approximately 130 A. After the step, the source current at node 3 increases with 25 A almost momentarily and settles at 163 A. The source currents at node 1 and 2 has a small increase to 134 A over 2 seconds. All three currents return to their initial value with the same response time for the other step.

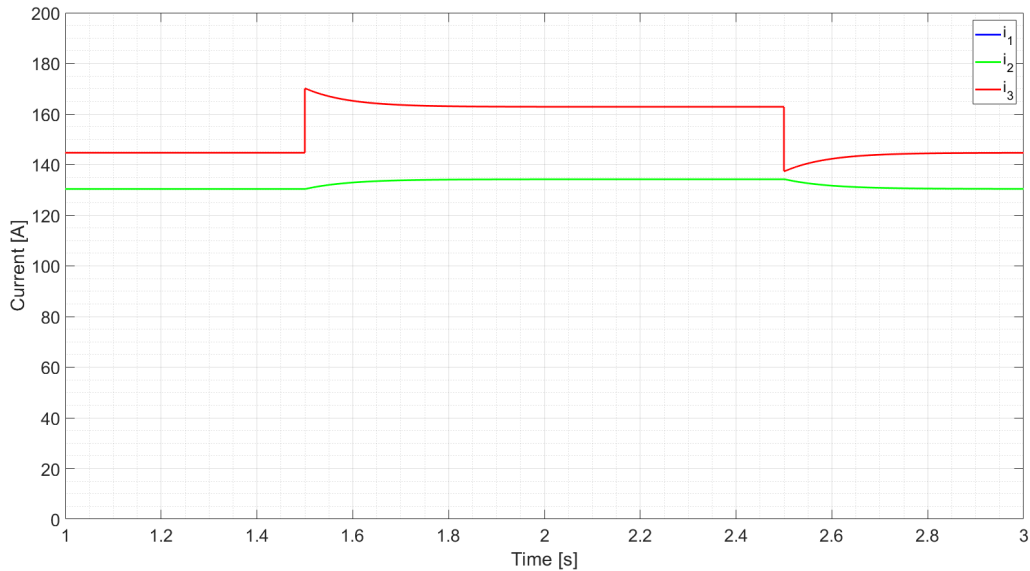


Figure 4.2: Response in source currents after a step of 10 kW at load 3 for the paper's microgrid.

4.1.3 Root Locus

To see how the stability is changed when changing the resistance and inductance of the lines, root locus plots are presented. Figure 4.3a shows the three eigenvalues moving to the left, from purple to yellow, when increasing the resistance from 0.9 to 1.1 times the nominal value with 100 steps. The two eigenvalues λ_2 and λ_3 are both presented in the shade around -1200 to -1100 on the real axis, while λ_1 is the one closest to origin. Since all three eigenvalues are moving to the left, the system is becoming more stable with higher resistance in the line.

Figure 4.3b shows the three eigenvalues moving to the right, from purple to yellow, when increasing the resistance from 0.9 to 1.1 times the nominal value with 100 steps. The two eigenvalues λ_2 and λ_3 are both presented in the shade around -1300 to -1050 on the real axis, while λ_1 is the one closest to origo. Since all three eigenvalues are moving to the right, the system is becoming less stable with higher resistance in the line.

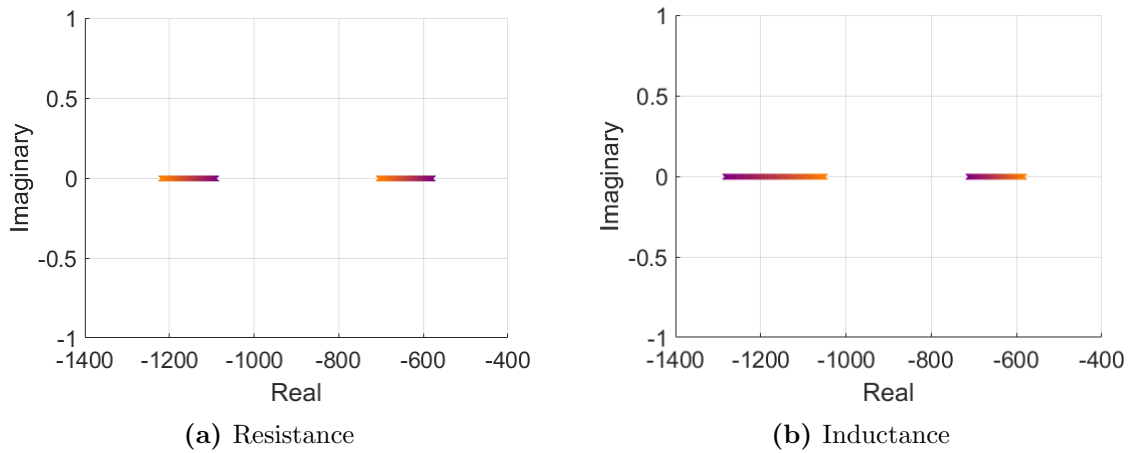


Figure 4.3: Change in eigenvalues for 0.9 to 1.1 times of nominal resistance and inductance value for the paper’s microgrid.

4.2 GridVille Representation

The focus of this chapter is to look at the behaviour of the GridVille microgrid to see if there is any parameters that should be changed to improve stability.

4.2.1 Line Currents

The first simulation of the GridVille microgrid is meant to find some of the same behaviour as the base microgrid. Therefore, in a step in the load node from 380 W to 480 W is performed to see the response of the lines between the producing nodes and the load node. Figure 4.4a show the state-space response of the three lines. Due to the different rated capacities and droop gains, the initial values of the currents are varying from 2.5 A for i_{14} to almost 3 A for i_{34} . After the step at 0.07 seconds, i_{14} has a slight overshoot, while i_{34} have a overdamped response. i_{24} has a response

in between those two mentioned, with an almost perfect response. The magnitude of the step for i_{34} is a bit higher than for i_{14} .

Figure 4.4b has the same initial values for the line currents as is in Figure 4.4a. After 7 seconds, the step is activated and all three line currents have approximately the same magnitude of the increase in current. All three currents have a near to perfect response and the same when going back to the initial load value after 13 seconds.

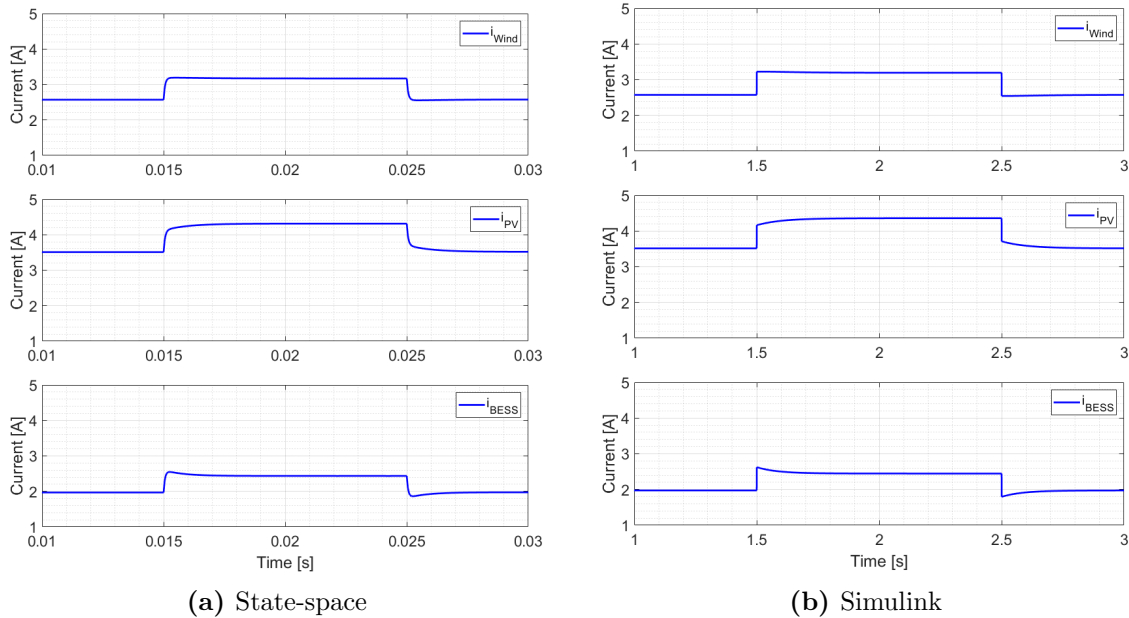


Figure 4.4: Response in line currents after a step of 100 W at load 4 for GridVille.

4.2.2 Root Locus

The same root locus analysis has been done for the GridVille microgrid, where the values of the resistance and inductance in the lines has been changed from 0.9 to 1.1 times the nominal value to see the change in eigenvalues. Figure 4.5a shows how the resistance moves to the left, from purple to yellow, when the resistance is increased. In the region of -700 to -850, λ_1 is placed, in the region -950 to -1500 λ_2 , while λ_3 starts is in the region -17000 and is therefore not visible in the plot.

For Figure 4.5b, the eigenvalues move to the right, from purple to yellow, when the inductance is increased. In the region of -700 to -850, λ_1 is placed, in the region -900 to -1100 λ_2 , while λ_3 starts is in the region -19000 to 15500 and is therefore not visible in the plot.

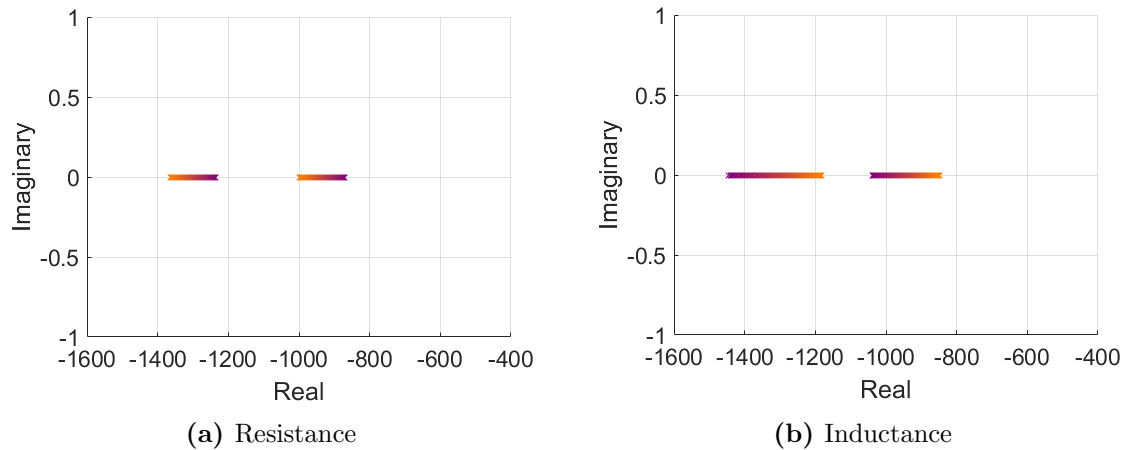


Figure 4.5: Change in eigenvalues for 0.9 to 1.1 times of nominal resistance and inductance value for GridVille.

4.2.3 350 W and 500 W Step in Load

To see how the microgrid behaves during a bigger step, a change in mode for the battery is performed. Figure 4.6a shows how the microgrid responds to a step from 500 W to 350 W at Node 4 where the PV power production at Node 1 and wind power production at node 2 stay are constant before and after the step, except for a small spike in production at the time of the step. The BESS goes from supplying power before 1.5 seconds, to not supplying or receiving any power after 1.5 seconds, where Node 1 and Node 2 produce enough by themselves.

In Figure 4.6b, the load goes from being disconnected to consuming the rated power of 500 W. The PV and wind power production then charges the battery with their power. After the step, the PV and wind production stays the same, except for the spike at the time of the step. The battery goes from charging to discharging and supplying the needed power to the load.

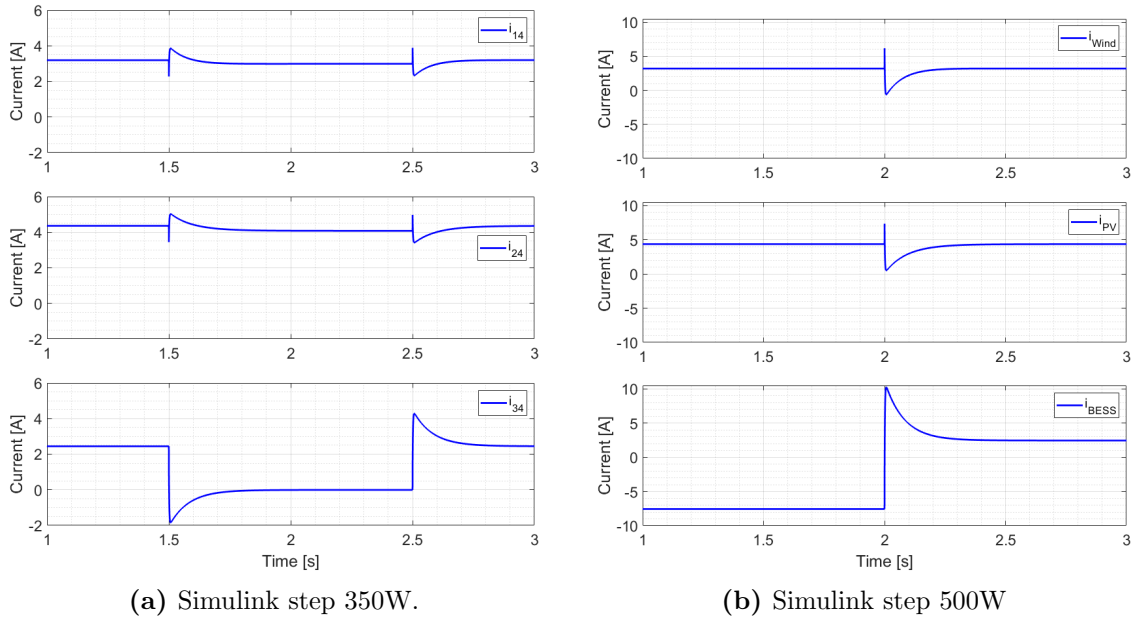


Figure 4.6: Load step at the load for GridVille.

4.3 Increasing the Voltage Level

This chapter will look at the response and stability of the GridVille microgrid when the voltage is increased. In Table 4.1, the change in eigenvalues are shown for the increase in voltage two, four and then times. Only λ_1 is presented since the two other eigenvalues λ_2 and λ_3 stay the same for all the four voltage levels. The trend is that the eigenvalue moves significantly to the right going from 48 V to 96 V, but the movement to the left decreases when increasing to 192 V and 480 V.

Table 4.1: λ_1 changing when increasing the rated voltage.

Rated Voltage [V]	48	96	192	480
λ_1	-17290	-14509	-13957	-13811

The impact on the participation factor can be seen in Equation 4.1. For this system, all the state variables has approximately the same affect on the corresponding eigenvalues as in the initial simulations with 48 V.

$$\mathbf{pf} = \begin{bmatrix} 0.332 & 0.336 & 0.332 \\ 0.317 & 0.053 & 0.630 \\ 0.351 & 0.612 & 0.038 \end{bmatrix} \quad (4.1)$$

The first observation in the step response in the plots in Figure 4.7a and 4.7b is that the current is much lower than the other plots because of the higher voltage delivering the same power. The response is however similar in shape and response time. The response for i_{Wind} is near to instant and with no overshoot for the Simulink model, but the state-space has a bit slower response and near to no overshoot. The

same instantaneous response is found for i_{PV} in the Simulink model, but the shape of the curve is underdamped. So it increases slowly towards the new equilibrium first rise. Also for the state-space model, the rise happens a bit slower, and slows down towards the end of the rise giving the overdamped characteristics. A slightly underdamped response can be seen for the i_{BESS} with the instantaneous rise from the Simulink model and slightly slower response for the state-space model.

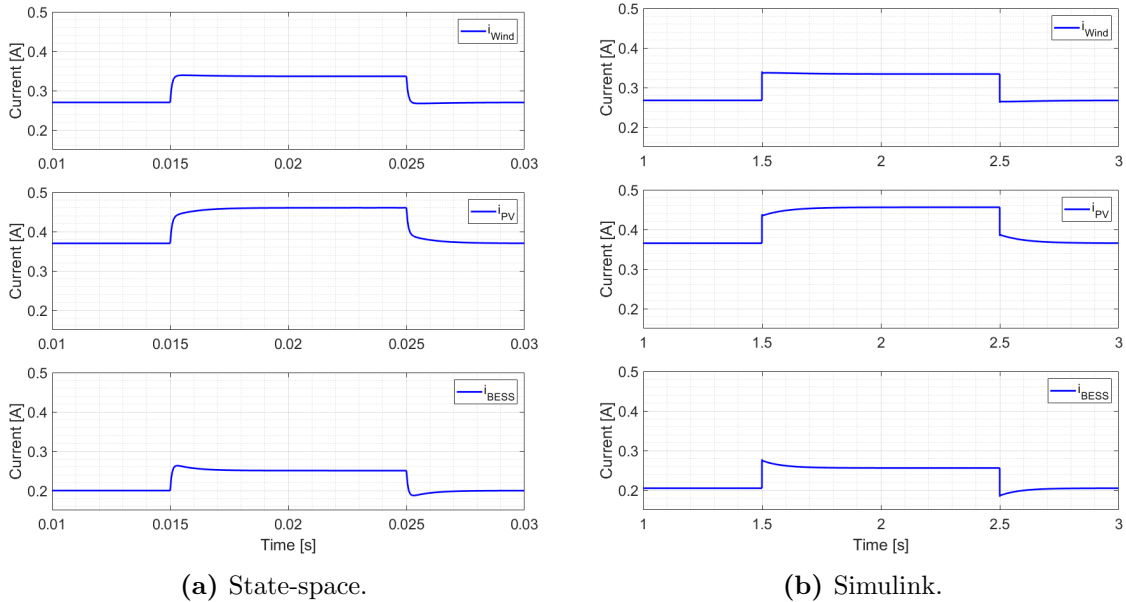


Figure 4.7: Load step of 100W with 480 V rated voltage for GridVille.

4.4 Changing the Droop Gain

In this subchapter, the simulations will investigate how the system stability and response to a step changes when changing the node's source power rating, and then the consequently the droop gains for the nodes. Table 4.2 shows the PV and Wind rated power which are lower than their original value. In this set, the BESS has a much higher rated capacity than the two other sources, unlike to the original scenario.

Table 4.2: Set1: Droop changing when changing the node's source rated power.

Node	PV	Wind	BESS
Rated Source Power [W]	500	500	3376
Droop Gains [Ω]	0.2	0.2	0.014

When calculating the eigenvalues with set 1 of droop gains, the result is shown Equation 4.2. All three eigenvalues are moving to the left, with λ_2 with the most movement, indicating a more stable system.

$$\lambda_1 = -17399 \quad \lambda_2 = -1485 \quad \lambda_3 = -954 \quad (4.2)$$

Looking at the effect of droop set 2 on the participation factor in Equation 4.3, the biggest change that the rightmost eigenvalues is now more affected by i_{BESS} , which in this case has the lowest droop value. The second eigenvalue is equally affected by i_{Wind} and i_{PV} , while eigenvalue 1 is affected the close to equally between the three state variables.

$$\mathbf{pf} = \begin{bmatrix} 0.344 & 0.500 & 0.156 \\ 0.344 & 0.500 & 0.156 \\ 0.312 & 0.000 & 0.688 \end{bmatrix} \quad (4.3)$$

One of the biggest differences between the scenario with changing the droop settings for the values in set 1 in Table 4.2, is the steady state value before and after the step. In this scenario, the highest starting current comes from the BESS at over just over 4 A, while the current from the Wind and PV power production are equal and at just under 2 A each. Both the PV and Wind response is a bit underdamped, where the response is faster for the Simulink model than the state-space model. The response for the BESS is overdamped and rises almost 1 A, while the other two nodes rise approximately 0.5 A each.

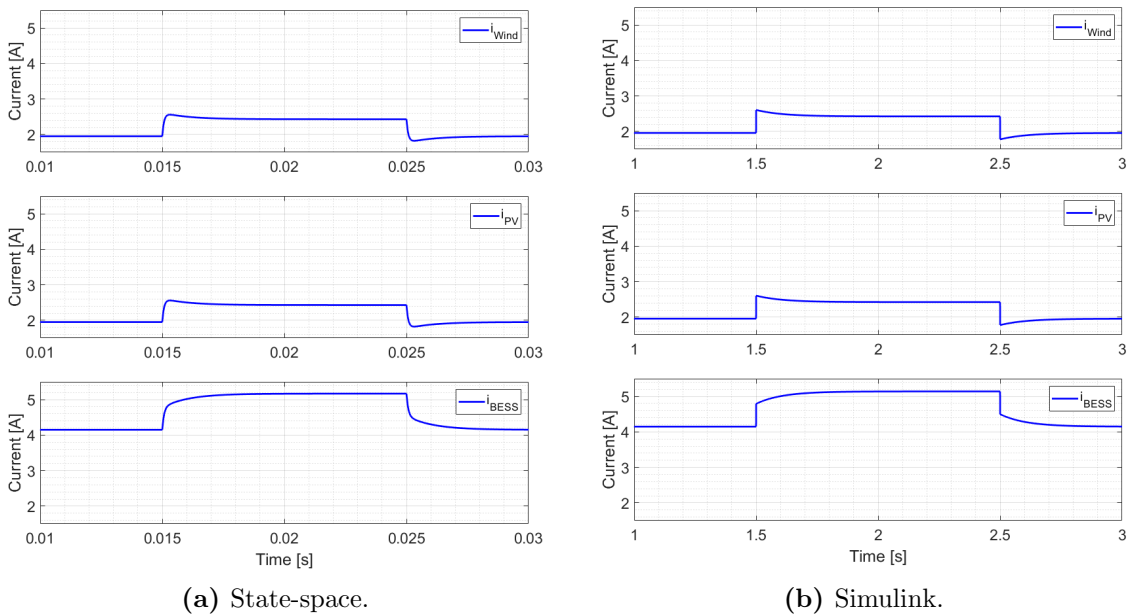


Figure 4.8: Load step of 100W with droop set 1 for GridVille.

The other set of rated source power at each node can be found in Table 4.3. In set 2, the rating is, as for set 1, equal for the Wind and PV node at 1900 W and a droop gain of 0.066Ω . The BESS has the same value for both rated voltage and droop gain as in the original case.

Table 4.3: Set 2: Droop changing when changing the node's source rated power

Node	PV	Wind	BESS
Rated Source Power [W]	1900	1900	576
Droop Gains [Ω]	0.066	0.066	0.19

For the eigenvalues in Equation 4.4, they have all shifted to the right after using the droop values in Table 4.3 to calculate the \mathbf{A} matrix. λ_2 moved the furthest to the right, but it is still not close to the y-axis.

$$\lambda_1 = -17265 \quad \lambda_2 = -1265 \quad \lambda_3 = -920 \quad (4.4)$$

In Equation 4.5, the resulting participation factor is shown.

Looking at the effect of droop set 2 on the participation factor in Equation 4.3, the biggest change that the rightmost eigenvalues is now more affected by i_{BESS} , which in this case has the lowest droop value. The second eigenvalue is equally affected by i_{Wind} and i_{PV} , while eigenvalue 1 is affected the close to equally between the three state variables.

$$\mathbf{pf} = \begin{bmatrix} 0.326 & 0.174 & 0.500 \\ 0.326 & 0.174 & 0.500 \\ 0.348 & 0.652 & 0.000 \end{bmatrix} \quad (4.5)$$

In Figure 4.9a and 4.9b, the state-space and Simulink model response, the Wind and PV responses are equal. Starting at 3 A and ending at 3.8 A for the Wind and PV current after the step with a slightly overdamped response, where the Simulink response rise faster at the time of the step. As the droop gain is equal to the original scenario for the BESS, the response is equal.

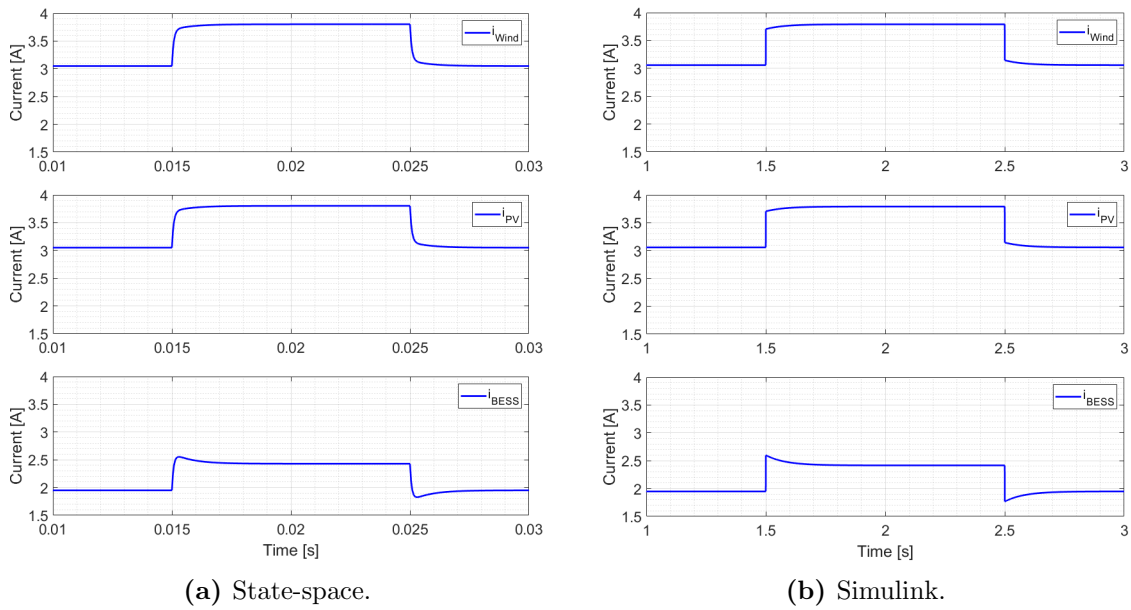


Figure 4.9: Load step of 100W with droop set 1 for GridVille.

4.5 Changing the Node Interconnections

To see if there the location of the nodes have any impact on the stability, different node structure will be investigated in this subchapter. First up, is the structure shown in Figure 4.10, where the line i_{12} from Node 1 is one meter and not connected to the load at Node 4, but the wind turbine at Node 2. i_{24} from Node 2 to Node 4 is the same, as is for Node 3 and i_{34}

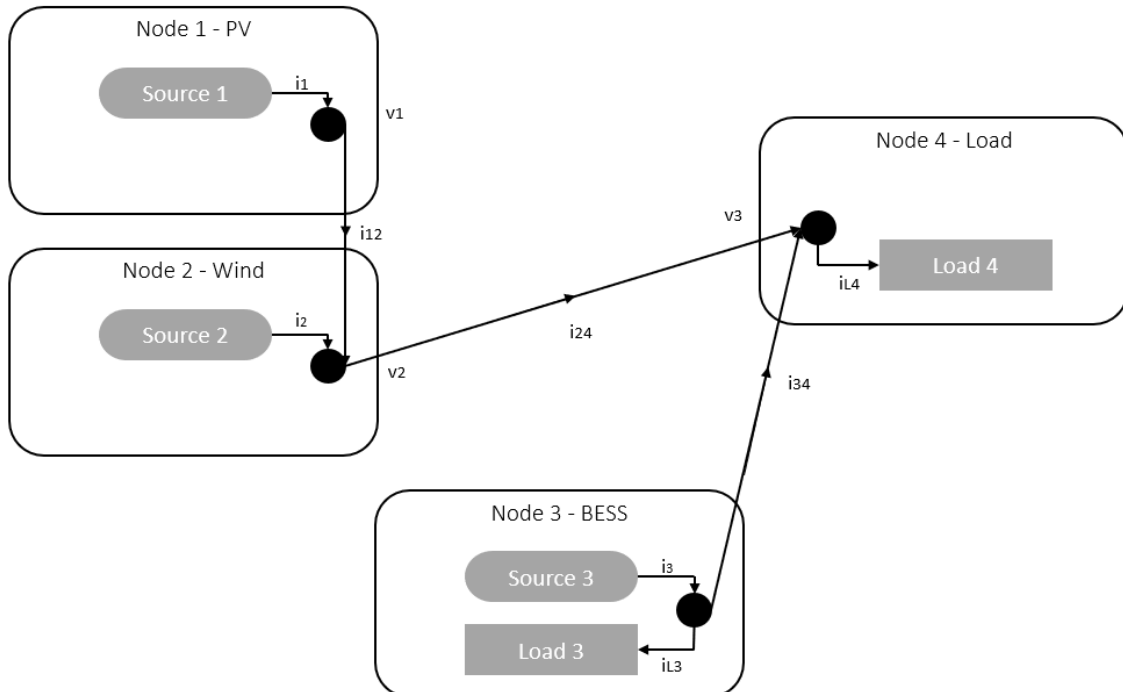


Figure 4.10: Overview of the microgrid of GridVille with interconnection set 1.

The changes made in the structure of the microgrid, as shown in Figure 4.10, results in a new incidence matrix \mathbf{M} for interconnection set 1 shown in Equation 4.6.

$$\mathbf{M} = \begin{bmatrix} 1 & -1 & 0 & 0 \\ 0 & 1 & 0 & -1 \\ 0 & 0 & 1 & -1 \end{bmatrix} \quad (4.6)$$

Running the script to get the new eigenvalues for this case gives the values in Equation 4.7. The first eigenvalue, λ_1 , moves so far to the left that it is a value to the power of two to the left. In other words, much longer to the left than the other two. Also λ_3 moves significantly to the left, by around then thousand. However, λ_2 moves to the right by 210, but it is still further to the left than the original case's rightmost eigenvalue.

$$\lambda_1 = -633600 \quad \lambda_2 = -1090 \quad \lambda_3 = -11890 \quad (4.7)$$

Looking at the effect of interconnection set 1 on the participation factor in Equation 4.3, the biggest change that the i_{Wind} only affects the first eigenvalue and the eigenvalue is only by i_{Wind} . State variable 2 and three affect the second and third eigenvalue almost the same amount.

$$\mathbf{pf} = \begin{bmatrix} 1.000 & 0.000 & 0.000 \\ 0.000 & 0.531 & 0.469 \\ 0.000 & 0.469 & 0.531 \end{bmatrix} \quad (4.8)$$

For the initial values, the wind power production is much lower than for the original case, going from just over 2.5 A to 1.5 A. The increase in current does not match the increase from the original scenario, therefore the PV and BESS has both a higher initial current and higher current after the step. In this simulations, the Simulink response for the Wind and PV power production has a spike at the time of the step, which goes down below the new steady state, before settling to the new steady state after about 0.3 seconds.

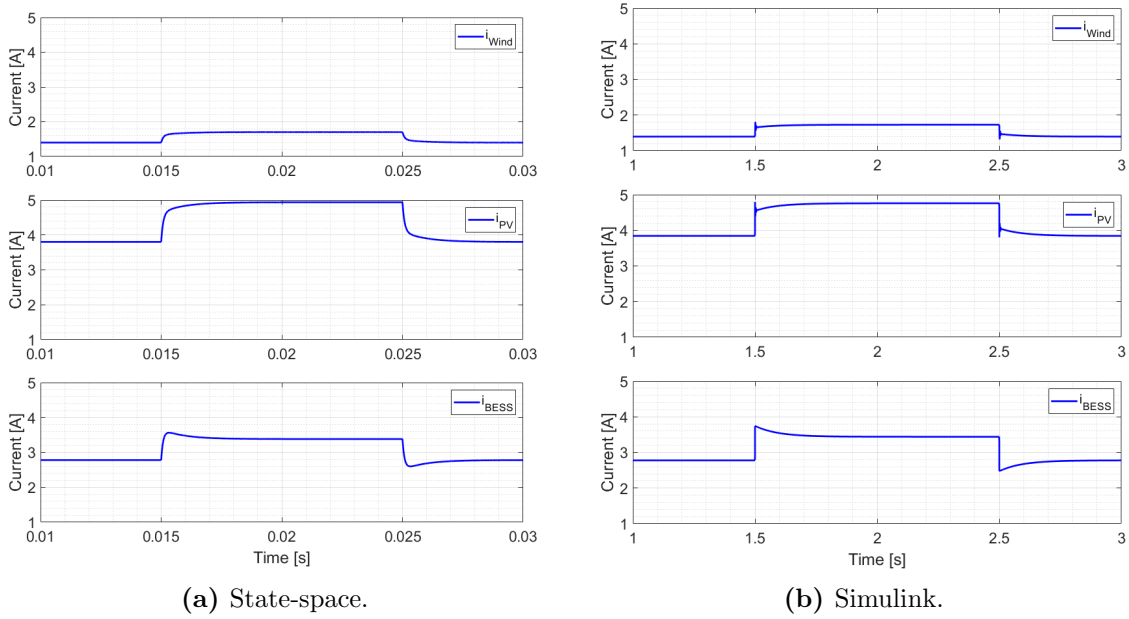


Figure 4.11: Load step of 100W with interconnection set 1 for GridVille.

The other structure of the microgrid that has been tested, is where additional lines between the three producing nodes are implemented. Figure 4.12 shows the additional lines of i_{21} and i_{23} between Node 2 and Node 1, and Node 2 and Node 3. These lines are assumed to have the same length as the others, 1 km, and giving the lines the same resistance and inductance as the three original lines.

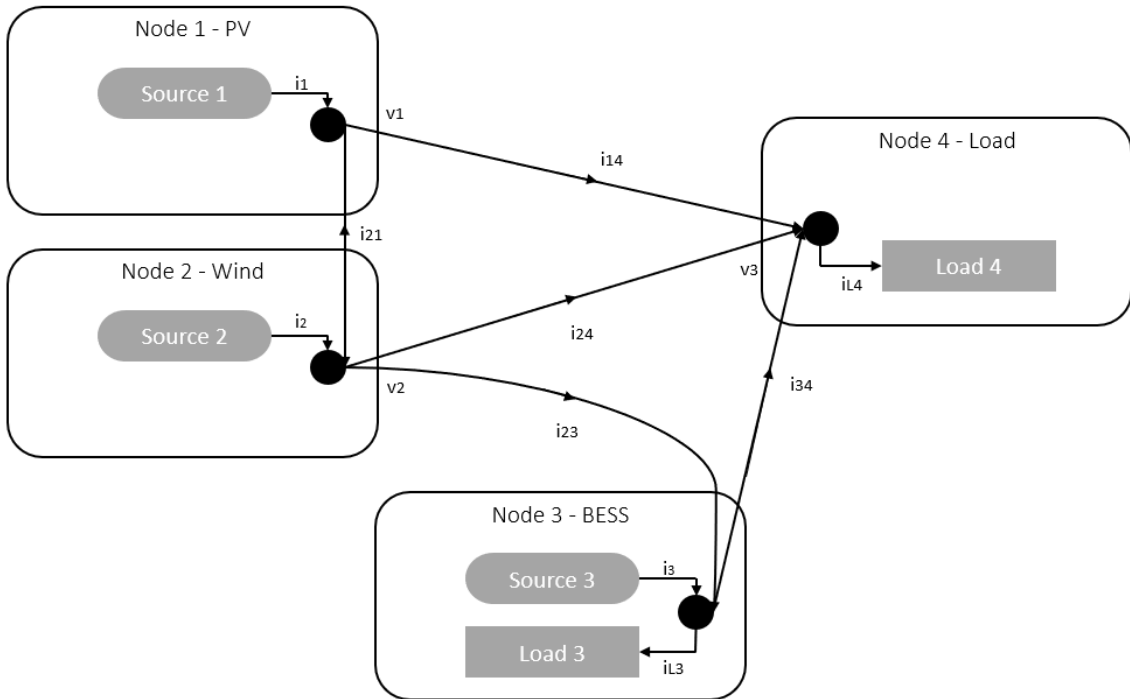


Figure 4.12: Overview of the microgrid of GridVille with interconnection set 2.

The corresponding incidence matrix \mathbf{M} for interconnection set 2, shown in Equa-

tion 4.9, takes the two extra lines into account. This makes the dimensions 5×5 , rather than 3×3 that the original scenario has.

$$\mathbf{M} = \begin{bmatrix} 1 & 0 & 0 & -1 \\ 0 & 1 & 0 & -1 \\ 0 & 0 & 1 & -1 \\ -1 & 1 & 0 & 0 \\ 0 & 1 & -1 & 0 \end{bmatrix} \quad (4.9)$$

The extra two lines gives two extra eigenvalues as can be seen in Equation 4.10. The two eigenvalues λ_4 and λ_5 are equal and compared to the eigenvalues further to the right in the original scenario, these two are over 300 further to the left than the original. That indicates a little less stable system than the original. Comparing λ_2 and λ_3 to the middle eigenvalue in the original scenario, these two are 700 and 1000 more to the left. For the eigenvalue furthest to the left, this scenario has a value over a thousand times more to the left than the original scenario.

$$\lambda_1 = -5863600 \quad \lambda_2 = -2700 \quad \lambda_3 = -2000 \quad \lambda_4 = -600 \quad \lambda_5 = -600 \quad (4.10)$$

For the participation factor, it is shown in Equation 4.11. The two additional lines i_{21} and i_{23} can be seen as the two additional rows. They affect the most the node that other state variables that they are connected to. The fifth state variable i_{23} and the third state variable i_{34} are affecting the fifth eigenvalue. The same trend could be found for the fourth and second state variable of i_{21} and i_{24} which affect the fourth eigenvalue the most. The third eigenvalue, which was mostly affected by the second state variable i_{24} is now also affected by the other lines that are connected to node to, the two additional state variables i_{21} and i_{23} .

$$\mathbf{pf} = \begin{bmatrix} 0.998 & 0.001 & 0.000 & 0.001 & 0.000 \\ 0.001 & 0.083 & 0.316 & 0.512 & 0.088 \\ 0.001 & 0.597 & 0.002 & -0.022 & 0.422 \\ 0.000 & 0.084 & 0.316 & 0.530 & 0.069 \\ 0.000 & 0.234 & 0.366 & -0.022 & 0.422 \end{bmatrix} \quad (4.11)$$

All the line current for the Simulink simulations are presented, where Figure 4.13a shown the three original lines and Figure 4.13b shows the two additional lines. The line carrying the current i_{14} has the same value and response as for the original scenario. i_{24} has a bit less current and i_{34} takes that difference and adds it to its current value. The additional line from Node 2 to Node 1 shows that around 0.5 A current goes is produced at the PV and goes to the Wind production node. A bit more is sent from the PV production to the BESS, around 0.8 A. The increase in current on those two lines are small. That means that The PV does not produce as much extra power to the other nodes, that is done by the Wind power production and BESS for their lines.

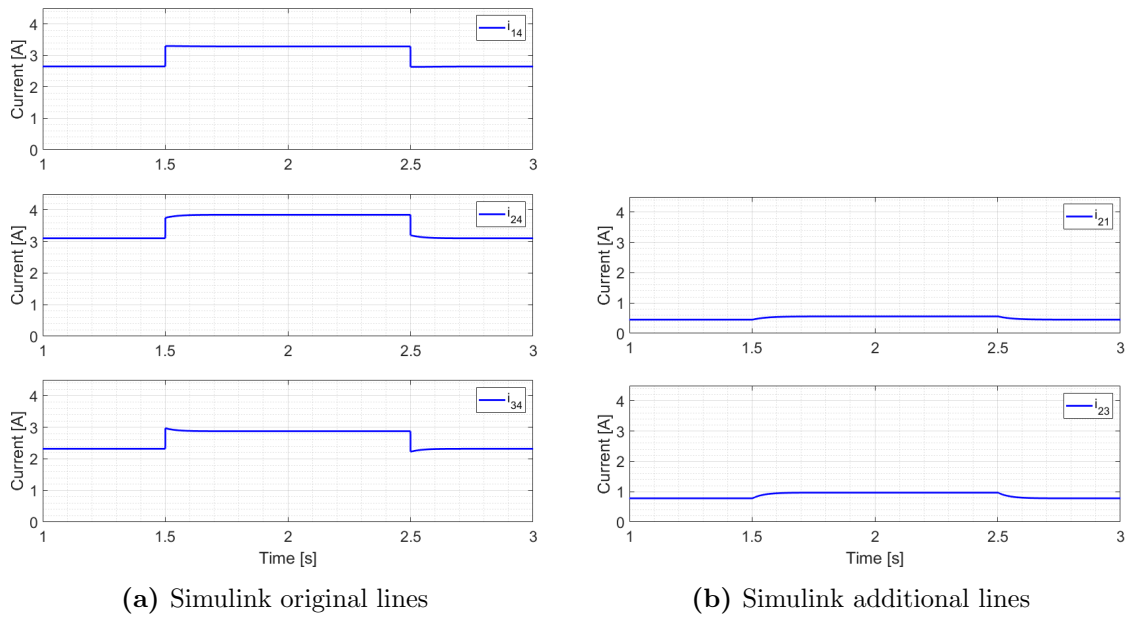


Figure 4.13: Load step of 100W with interconnection set 2 for GridVille for Simulink.

The difference between the Simulink representation in Figure 4.13 and Figure 4.14 are relatively big. i_{14} in Figure 4.14a has the same initial value as the Simulink model, but the state-space model overshoots a lot before reaching the new steady state value. There is a much slower response for i_{24} and i_{34} compared to the Simulink response 0.002 s. The response of the two additional lines in Figure 4.14b

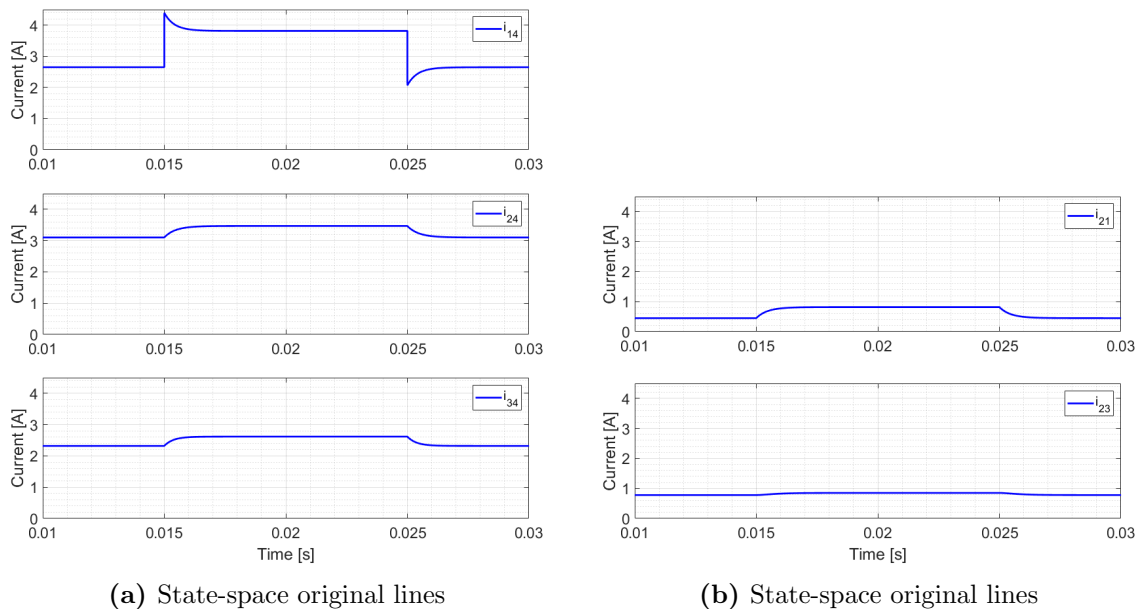


Figure 4.14: Load step of 100W with interconnection set 2 for GridVille for state-space.

4.6 Changing the Load Distribution

In this chapter, the effect on stability when changing the number of loads will be investigated. In Figure 4.15, the load has been split in two, so that there is an additional load at Node 2 of 250 W and the load at Node 4 has been decreased to 250 W, adding up to the original load. Note that the load at node 3 is only representing the charging of battery, not, an actual load.

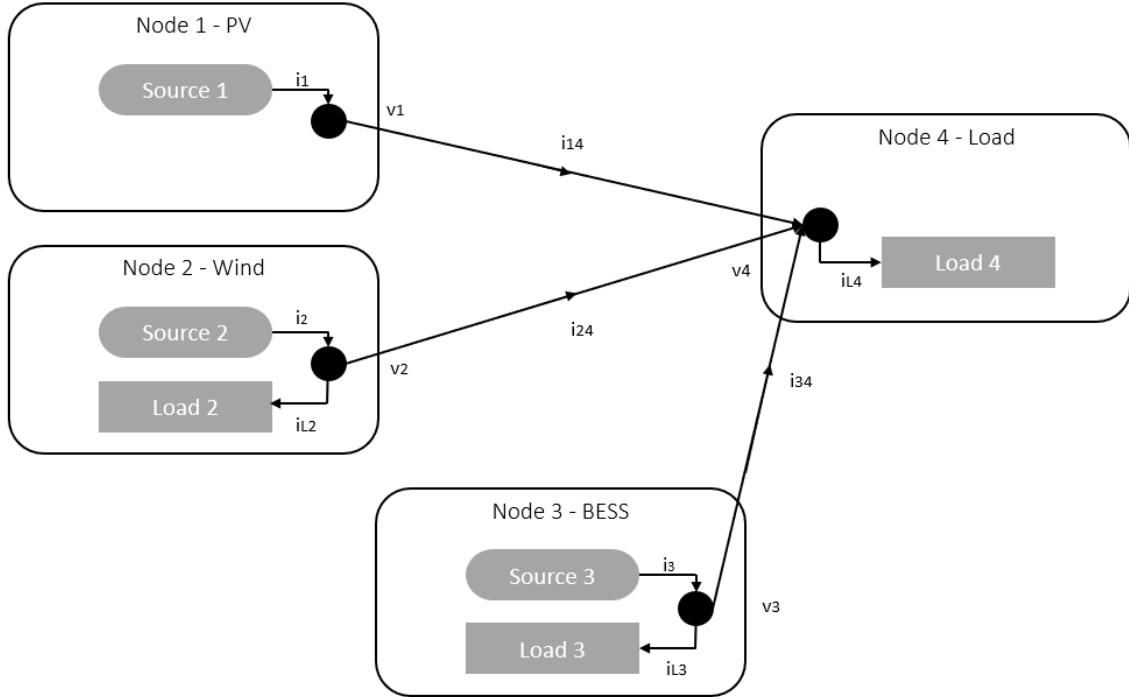


Figure 4.15: Overview of the microgrid of GridVille with load distribution set 1.

When calculating the eigenvalues with the load conductance matrix \mathbf{G} with the extra parameter of g_{l2} and reduced g_{l4} , the result is shown in Equation 4.12. Both λ_2 and λ_3 are exactly the same as the original scenario. However, λ_1 is almost 2000 further to the right.

$$\lambda_1 = -15323 \quad \lambda_2 = -1300 \quad \lambda_3 = -935 \quad (4.12)$$

Equation 4.13 shows the participation factor with load distribution set 1 does not affect the matrix significantly.

$$\mathbf{pf} = \begin{bmatrix} 0.332 & 0.334 & 0.334 \\ 0.319 & 0.053 & 0.628 \\ 0.349 & 0.614 & 0.038 \end{bmatrix} \quad (4.13)$$

This load structure makes the line currents lower than the original scenario, as can be seen in Figure 4.16a and 4.16b. All currents have a lower initial value and

have a lower increase after the step. The only difference between the Simulink and state-space model is that the Simulink model is faster in the response.

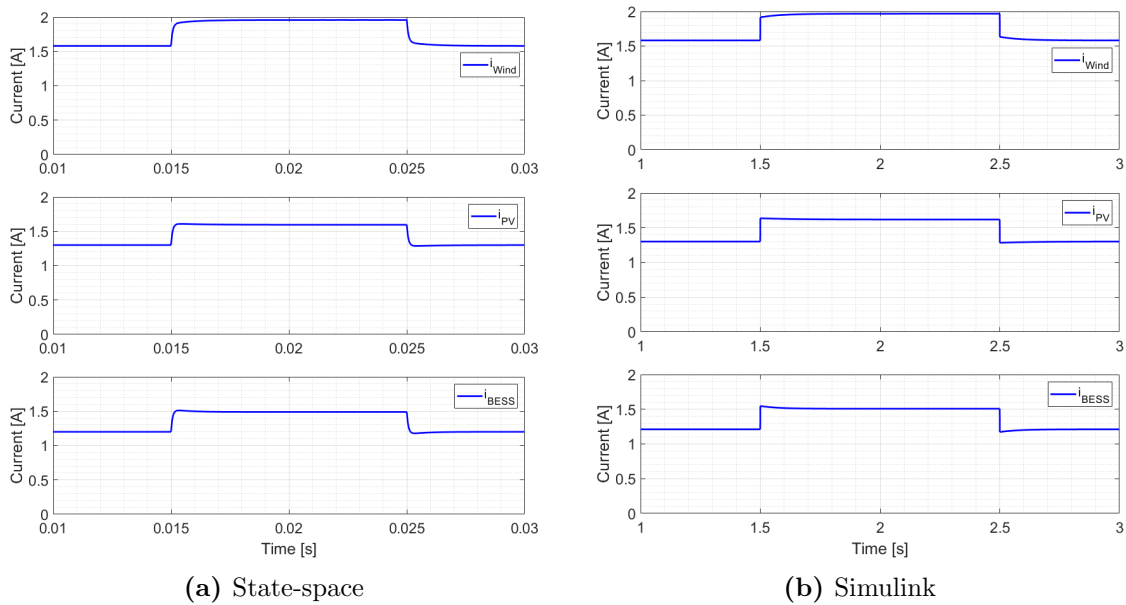


Figure 4.16: Load step of 100W with load distribution set 1 for GridVille.

To try another load structure, all the nodes was given an equal load of 125 W. This can be seen in Figure 4.17. Note that the load at node 3 is an actual load and not the charging of the battery.

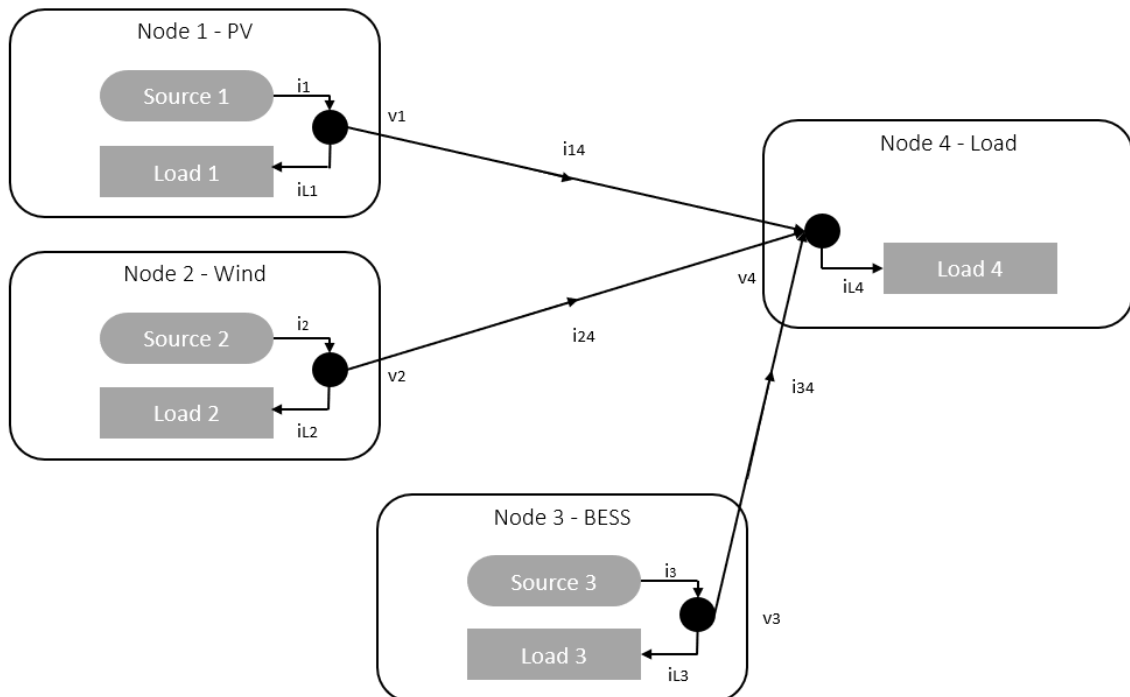


Figure 4.17: Overview of the microgrid of GridVille with load distribution set 2.

The effect on the eigenvalues are shown in Equation 4.14, where λ_3 and λ_2 are 1

and 6 to the left, almost the same as the original scenario. λ_1 is almost 3000 to the right.

$$\lambda_1 = -14513 \quad \lambda_2 = -1306 \quad \lambda_3 = -936 \quad (4.14)$$

Equation 4.15 shows the participation factor with load distribution set 2 does not affect the matrix significantly.

$$\mathbf{pf} = \begin{bmatrix} 0.332 & 0.334 & 0.334 \\ 0.318 & 0.053 & 0.629 \\ 0.350 & 0.613 & 0.037 \end{bmatrix} \quad (4.15)$$

The resulting line currents consequently much lower than the original scenario because there is less need to deliver power to the load node. In Figure 4.18a i_{Wind} starts at just over 0.5 A and increased by 0.1 A after the step. i_{PV} started at just over 2.5 A and rises to nearly 2 A, but with a longer response time than the other two line currents. The most change compared to the original scenario is the i_{BESS} , which has a small spike after the step, but stabilises again at the same value as before the step. For the Simulink response in Figure 4.18b, the response is similar, but just a bit faster.

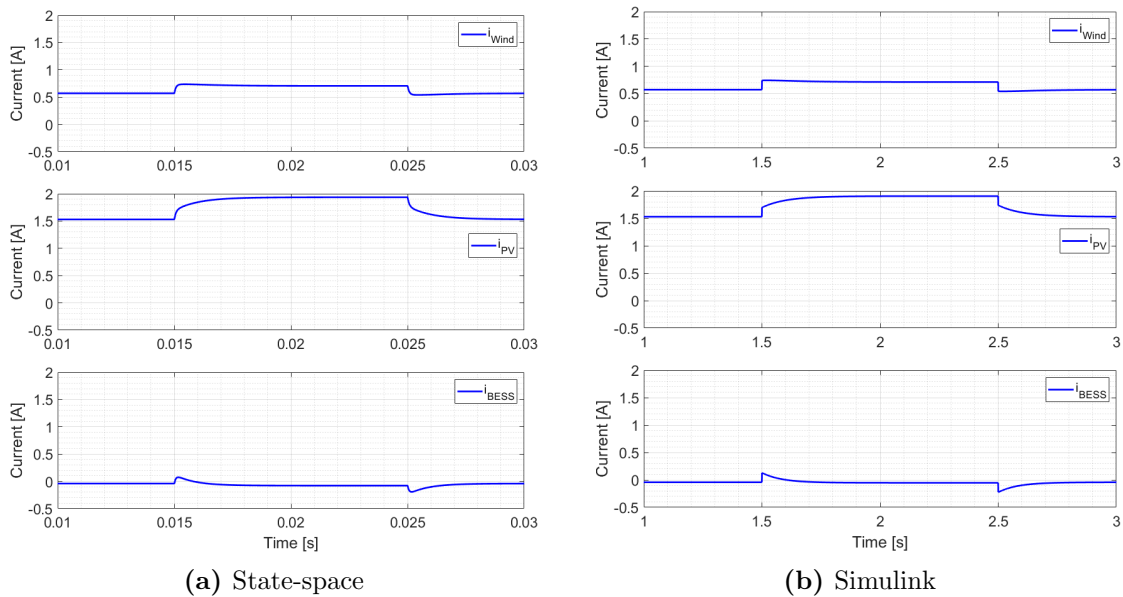


Figure 4.18: Load step of 100W with load distribution set 2 for GridVille.

5 Discussion and Conclusion

This chapter will summarise the trends showed in the results chapter in section 4 and comment on their effect on the changes in voltage, droop gain, interconnection lines and load distribution. After that, the practical suggestions will be presented and the final conclusion will be elaborated. In addition, there will be discussed some improvements for potential further work.

5.1 Comparison to the Paper

For the state-space simulation of the paper, it corresponds to the one in the paper. The time step of the Simulink simulations are 100 times slower, and not as fast as the indicated response in the paper. However, the shape of the response matches the one in the state-space simulations. Also the source current plot have the same issue with the much slower response than in the paper, but the response is near to identical to the paper. The eigenvalues produced in this thesis is almost the same as the one in the paper, the only difference could be the round-off errors. For the root locus plots of the change in resistance and inductance, they are also close to identical as in the paper. With the note that the Simulink simulations are slower indicated in the paper, the recreation of the paper's model and results have been successfully done and it can be used to see if the GridVille's results are realistic or not.

The GridVille microgrid was implemented in Simulink and state-space to be as close to the paper as possible. The biggest difference is that each node only functions as either a supplier or consumer of power, not both. That makes the line currents equal to the source currents and it is also visible in the characteristics to the line currents. The currents reaches the new steady state faster than the paper line current response. The response of the GridVille representation is closer in shape and response time as the source currents of the paper. In addition, eigenvalues are placed more to the left and the root locus plots of the resistance and inductance are similar to the papers response. This means that the GridVille microgrid have the same characteristics as the paper and can therefore be seen as plausible.

Another problem with the difference between the model of the paper and GridVille is that the GridVille model does not have constant power loads. When trying to simulate it with the GridVille specifications in Simulink, errors would occur that was solved by changing the loads to resistive loads. That makes the loads a bit less accurate, but the resistance values have been calculated to consume the same power at the steady state value. By running the simulations long enough to reach steady state before the step, the plots and responses seems not too affected by the more inaccurate load when comparing them to the state-space simulations, which have constant power loads, for the corresponding cases and when comparing the initial GridVille plots.

The case with the most variation between the state-space simulations and the Simulink simulations, is for the second case with interconnections changes. That may

be the simulations where the resistive loads are the most noticeable, where the state-space simulations follows the same pattern and curves as the previous simulations, but the Simulink has a much different slopes on the state-space and previous simulations.

The participation factor difference from the paper to GridVille shows that the third and rightmost eigenvalue goes from being affected by all three state variables to being dominated by the second and affected a bit by the second and first state variable. It seems that the GridVille microgrid has a quicker response and more stable than the paper.

For simplicity, the same line has been used for the GridVille as for the paper. This line is dimensioned for a max current of 200 A, which fits the paper well. However, the GridVille microgrid do not have as high currents, they are almost 20 times lower. If another line had been chosen, the resistance and inductance would have been different and it could have affected the results.

For the producing nodes, Node 1 with the wind power production and Node 2 with the PV power production, they are changing the power delivered to the system during the simulations. In the real world, they would not be able to do that, just produce constant power and the battery would balance the power difference. The step response of 350 W and 500 W does show that it is possible to run the simulations forcing the PV and Wind current to the BESS after a step change in load, but because of the spike in current at the step, it is still not a perfect representation. However, in these simulations, the point is not to make it as realistic as possible, but to see if the system as a whole is stable.

Node 4 had a droop setting of 1Ω because that indicates a very small source and needed to be there for the simulations to run. Errors would occur in the simulations if it was set to zero. This means that there is a difference in the representation between the two simulation model, but since it is as small as it is, it seems to be negligible.

5.2 Stability Analysis

This part of the discussion will focus on the potential improvements of the GridVille microgrid. All the four changes in parameters will be discussed to see if there are some possible gains in terms of stability.

5.2.1 Increasing the Voltage Level

The first change in the parameters done was increasing the voltage. The leftmost eigenvalue moved quickly to the right. However, it was far away from the two other rightmost eigenvalues, which were not affected by the increase in voltage. Nor the participation factor was affected, and this indicate that there the increase in voltage does not increase the stability of the system. On the other hand, the benefit for increasing the voltage is less loss in the lines because of lower currents, and it

could therefore also mean that GridVille could buy cheaper lines between the nodes. Therefore, it could be a good choice to increase the voltage because the gain in less loss is bigger than the slightly less to the leftmost eigenvalue.

5.2.2 Changing the Droop Gain

The next change of parameters was changing the droop gain by changing the rated source power. The higher rated power, the lower droop gain, which gives a higher current. The downside of having with this is that the response tend to be slower to the new steady state value. When the power rating is lower, that gives a higher droop gain. Consequently, the current supplied is lower and response is faster than the with a bit of overshoot.

Set 1 of the droop changes consist of one big source and two smaller, while Set 2 has two equal big sources and one smaller. When having one big source and two smaller, the eigenvalues move to the left. The participation factor goes from the third state variable having almost all impact on the rightmost eigenvalue in Set 1, to sharing the impact equally between the first and second state variable in set 2. The rightmost eigenvalues goes from the third to second and the total affect is the It could indicate that it is better to have one dominating producer with some smaller nodes. It could also mean that having different power sources in one node could be better than having them separated. However, that could be difficult when it comes to having optimal solar and wind conditions at one location. Another solution could be to have smaller batteries at each producing node to reduce the number of nodes and decrease the length the current need to travel before being stored and potentially increase stability and lower power losses. Another suggestion is to have a bigger battery and smaller power sources, but that have to be investigated further.

5.2.3 Changing the Node Interconnections

The third change in parameters was meant to see if the microgrid structure could affect the stability of the system. There are many possibilities, but in this thesis only two grid connections were checked. Those two could represent a simpler grid, the first case, and a more complex grid connection.

The simpler grid, interconnection set 1, was fundamentally connecting the two power producing sources PV and Wind. The overall movement of the eigenvalues was to the left, especially for 1 and 3. However, eigenvalue 2 moves to the right, but not more than the rightmost eigenvalue, meaning that set 1 is a bit more stable than the original case. The participation factor shows that the influential state variable goes from the first and second to the second and third. The second interconnection set gives two additional lines seen in case 2 in the system between the three supplying nodes have increased the number of eigenvalues with two. The two rightmost eigenvalues are more to the right than the original, meaning a less stable system and less responsive. The increased complexity in the system seems to not pay of with more stability. Even though it does not have a big impact, it seems as the less complex grid is more stable and that it could pay off. However, the reliability concern could

make this a choice if the goal is to operate normally if one or two lines taken out. Another positive remark with keeping the grid simple is that it would be cheaper to build and it would possibly make troubleshooting easier for the grid.

5.2.4 Changing the Load Distribution

The final change in parameters was done by changing the distribution of the 500 W of load over the four nodes. The first rearranging of the load is two 250 W loads, One at Node 4 and one at Node 2. When simulating that scenario, the all currents in the lines are decreased and the response is close to perfect for both the state-space and. The only eigenvalue to move is the leftmost, which is still by far the leftmost eigenvalue and the participation factor does not change.

When giving every node a load of 125 W each, line currents from the smaller power supplier as the Wind at Node 1 and the BESS at Node 3, drops significantly, and the PV at Node 2 takes a bigger portion of supplying Node 4. The current from the BEES stays close to zero for the steady state, except for some spikes at the steps. The two rightmost eigenvalues moves slightly to the left, and the leftmost to the right, but is still far from the two other eigenvalues, while the participation factor is unchanged.

When looking at the response and the eigenvalues it could increase the stability if the load was distributed around the nodes, however, the eigenvalues does not move that significantly and it is therefore hard to suggest something here. This may be difficult because the loads will be at specific locations in the village and may not be at one of the production sites. However, it could be interesting to investigate if one of the production nodes, the PV power production may be the most relevant, to set with the load.

5.3 Further Work

For further work on the microgrid of GridVille, the specialisation project the semester before could have the objective of designing each converter individually and analyse them. Then, the master thesis could consider the connected microgrid where all the converters are working together. After the summer, GridVille have come further in the planning and this could be a natural starting point. Designing the converters analytically, developing the individual models in Simulink developing could be a suitable preparation for the master thesis. Then the master thesis could use the developed converters and Simulink files, and connect them together and analyse that system with small signal analysis.

Each converter could be connected to their respective power source and simulate different scenarios. Using the PV block and a controlled voltage source for the wind turbine, it is possible to use the different irradiance values for different and wind speed values to see how the BESS should be operated. The values can be changed between different seasons, weather conditions and scenarios.

Since the development could have come further for GridVille, it could be an idea to have the master student work on the specific simulation files, and possibly work together with the GridVille volunteers. That could be beneficial for both the master student and the volunteers. The master student faster be introduced to the theory and simulation files needed, and when trouble and questions, the master student could discuss and solve the problems together. Since the thesis is cooperation, the cooperation between the master student and the volunteers in GridVille should be a priority. Both parts would gain from that. In that way, it would be easier to transfer the knowledge of the results of the thesis and for the next.

5.4 Conclusion

This thesis has looked at the stability properties of a representation of the GridVille microgrid with Simulink simulations and state-space analysis. After investigating and recreating the paper *Reduced-order model and stability analysis of low-voltage DC microgrid* and making the GridVille representation through the steps of the paper to have some foundation to compare the results against.

To sum up the possible improvements for the GridVille Microgrid with the results of this thesis, the following is suggested:

- Increase the voltage.
- One bigger power source is better than two equally big.
- Reduce the number of nodes.

The first point, increasing the voltage, does not affect the stability directly, but the currents become smaller, and thus the losses on the lines become lower without reducing the stability of the system. For the second and third point, the suggestion is directed towards either dividing the loads or BEES to each node, or join together power sources. Reducing the number of nodes and lines would increase the stability, and could also reduce power losses and the cost of the lines. However, these suggestions may not be realisable because of the needed solar and wind conditions for production, and where the load can be placed in the village. An easier way for this to be realised is to put the battery at one of the other nodes, or divide it into smaller batteries and have it spread on different nodes.

Bibliography

- [1] Kjell Petersen Synstad. ‘The Specialisation Project’. In: *Project report in TET4510*. Department of Electric Power Engineering, NTNU - Norwegian University of Science and Technology. Dec. 2021.
- [2] UN. *Ensure access to affordable, reliable, sustainable and modern energy*. URL: <https://www.un.org/sustainabledevelopment/energy/> (visited on 26th May 2022).
- [3] Brandon A Bridge, Dadhi Adhikari and Matias Fontenla. ‘Electricity, income, and quality of life’. In: *The Social Science Journal* 53.1 (2016), pp. 33–39.
- [4] Todd Levin and Valerie M Thomas. ‘Can developing countries leapfrog the centralized electrification paradigm?’ In: *Energy for Sustainable Development* 31 (2016), pp. 97–107.
- [5] Sivapriya Mothilal Bhagavathy and Gobind Pillai. ‘PV microgrid Design for Rural Electrification’. In: *Designs* 2.3 (2018).
- [6] Shailendra Kumar Jha, Petter Stoa and Kjetil Uhlen. ‘Green and hybrid microgrid for rural electrification’. In: *2016 IEEE Region 10 Humanitarian Technology Conference (R10-HTC)*. IEEE. 2016, pp. 1–5.
- [7] Teknisk ukeblad. *NTNU skal blir mer bærekraftig, men petroleumsfaget består: – Vårt oppdrag er å utdanne studenter til norsk arbeidsliv*. URL: <https://www.tu.no/artikler/ntnu-skal-bli-mer-baerekraftig-men-petroleumsstudiet-bestaar-vart-oppdrag-er-a-utdanne-studenter-til-norsk-arbeidsliv/486271> (visited on 4th June 2022).
- [8] NTNU. *Kunnskap for en bedre verden - NTNU strategi 2018-2025*. URL: <https://www.ntnu.no/ntnus-strategi> (visited on 26th May 2022).
- [9] Sandeep Anand and Baylon G Fernandes. ‘Reduced-order model and stability analysis of low-voltage DC microgrid’. In: *IEEE Transactions on Industrial Electronics* 60.11 (2012), pp. 5040–5049.
- [10] Panagiotis Kofinas, George Vouros and Anastasios I Dounis. ‘Energy management in solar microgrid via reinforcement learning’. In: *Proceedings of the 9th Hellenic Conference on Artificial Intelligence*. 2016, pp. 1–7.
- [11] Samir M Dawoud, Xiangning Lin and Merfat I Okba. ‘Hybrid renewable microgrid optimization techniques: A review’. In: *Renewable and Sustainable Energy Reviews* 82 (2018), pp. 2039–2052.
- [12] R Martinez-Cid and E O’Neill-Carrillo. ‘Sustainable microgrids for isolated systems’. In: *IEEE PES T&D 2010*. IEEE. 2010, pp. 1–7.
- [13] Salvatore D’Arco, Jon Are Suul and Marta Molinas. ‘Implementation and Analysis of a Control Scheme for Damping of Oscillations in VSC-Based HVDC Grids’. In: *2014 16th International Power Electronics and Motion Control Conference and Exposition*. IEEE. 2014, pp. 586–593.
- [14] JA Pecas Lopes, Carlos L Moreira and AG Madureira. ‘Defining control strategies for microgrids islanded operation’. In: *IEEE Transactions on power systems* 21.2 (2006), pp. 916–924.

- [15] Chandra Bajracharya et al. ‘Understanding of tuning techniques of converter controllers for VSC-HVDC’. In: *Nordic Workshop on Power and Industrial Electronics (NORPIE), June 9-11, 2008, Espoo, Finland*. Helsinki University of Technology. 2008.
- [16] Nagaraju Pogaku, Milan Prodanović and Timothy C. Green. *Modeling, Analysis and Testing of Autonomous Operation of an Inverter-Based Microgrid*. IEEE, 2007.
- [17] Magdi Sadek Mahmoud, S Azher Hussain and Mohammad Ali Abido. ‘Modeling and control of microgrid: An overview’. In: *Journal of the Franklin Institute* 351.5 (2014), pp. 2822–2859.
- [18] Naser Mahdavi Tabatabaei, Ersan Kabalci and Nicu Bizon. *Microgrid Architectures, Control and Protection Methods*. Springer, 2019.
- [19] Mostafa Farrokhhabadi et al. ‘Microgrid Stability Definitions, Analysis, and Examples’. In: *IEEE Transactions on Power Systems* 35.1 (2019), pp. 13–29.
- [20] Jan Machowski et al. *Power System Dynamics: Stability and Control*. John Wiley & Sons, 2020.
- [21] Varshan Erik Shankar. *Personal communication*. Last read: 2022-04-20.
- [22] Mohan N. Undeland, William P. Robbins and N. Mohan. ‘Power Electronics: Converters, Applications and Design’. In: *Converters, Applications, and Design*. John Wiley & Sons, 2003.
- [23] Liqun Shang, Hangchen Guo and Weiwei Zhu. ‘An improved MPPT control strategy based on incremental conductance algorithm’. In: *Protection and Control of Modern Power Systems* 5.1 (2020), pp. 1–8.
- [24] Kåre Bjørvik and Per Hveem. *Reguleringsteknikk*. Kybernetes forlag, 2014.
- [25] Xiaonan Lu et al. ‘Hierarchical control of parallel AC-DC converter interfaces for hybrid microgrids’. In: *IEEE Transactions on Smart Grid* 5.2 (2013), pp. 683–692.
- [26] Mohammad Amin. ‘Small-signal Stability Characterization of Interaction Phenomena between HVDC System and Wind Farms’. In: (2017).
- [27] Prabha Kundur et al. ‘Definition and Classification of Power System Stability IEEE/CIGRE joint task force on stability terms and definitions’. In: *IEEE transactions on Power Systems* 19.3 (2004), pp. 1387–1401.
- [28] MathWorks. *What Are State-Space Models?* URL: <https://se.mathworks.com/help/ident/ug/what-are-state-space-models.html> (visited on 7th June 2022).
- [29] Erik Cheever. *State Space Representations of Linear Physical Systems*. URL: <https://lpsa.swarthmore.edu/Representations/SysRepSS.html> (visited on 7th June 2022).
- [30] Franco Garofalo, Luigi Iannelli and Francesco Vasca. ‘Participation factors and their connections to residues and relative gain array’. In: *IFAC Proceedings Volumes* 35.1 (2002), pp. 125–130.

